7-2021

The Balance of Excitation and Inhibition and Its Influence on Cortical States and Rett Syndrome

Jingwen Li
University of Arkansas, Fayetteville

The Balance of Excitation and Inhibition and Its Influence on Cortical States and Rett Syndrome

A dissertation submitted in partial fulfillment
of the requirements for the degree of
Doctor of Philosophy in Physics

by

Jingwen Li
Beijing Normal University
Bachelor of Science in System Science, 2013
Beijing Normal University
Master of Science in System Theory, 2016

July 2021
University of Arkansas

This dissertation is approved for recommendation to the Graduate Council

---

Woodrow L. Shew, Ph.D.
Dissertation Director

Pradeep Kumar, Ph.D.
Committee member

Erica Westerman, Ph.D.
Committee member

ABSTRACT

Our brain consists of billions of neurons, properly coordinating to process information and realize brain functions. Among them, there are two types of neurons: excitatory neurons and inhibitory neurons. The firing of excitatory neurons increases the membrane potential of downstream neurons, and thus excites other neurons to fire. The firing of inhibitory neurons, in contrast, decreases the membrane potential of downstream neurons, and thus inhibits other neurons to fire. The interplay of excitatory and inhibitory neurons shape the spiking activity in the population. Thus, the 'balance of excitation and inhibition' plays an important role in cortical processing and brain functions. An imbalance towards either excitation or inhibition leads to dysfunctional circuit mechanisms, and is related to many brain disorders. Here, we explore the influence of the balance of excitation and inhibition on cortical states and a devastating neurodevelopmental disorder - Rett syndrome (RTT). In Chapter 1, we built a family of models where varying the ratio of inhibitory synaptic strength relative to excitatory synaptic strength tunes the network dynamics to two possible cortical states - criticality and asynchronous dynamics. And our work shows that the two distinct and competing scenarios can be generated in the same neural system, when the excitation and inhibition are properly balanced. In Chapter 2, we studied how the RTT-related imbalance of excitation and inhibition influences cortical dynamics and motor function in freely behaving rats by comparing normal rats with a transgenic rat model of RTT. Our results suggest that excessive inhibition in RTT gives rise to an excessive synchrony in primary motor cortex, which is related to stereotyped intracortical and cortex-body interactions and less complexity in movement.

DEDICATION

This dissertation is dedicated to my mother.

ACKNOWLEDGEMENTS

I would like to express my sincerest gratitude to my advisor, Dr. Woodrow Shew, for his invaluable guidance and continuous support not only in academia, but also in every aspect of my life. Without him, I would not have enjoyed my research this much and come over many difficulties during my PhD study. I could not have asked for a better mentor.

I would like to thank the past and present members in my committee for giving me constructive criticisms and suggestions on my work. Thanks to our postdoc, Dr. Shree Gautam, for instructing me and helping me with surgeries and animal care. Thanks to my labmate, Patrick Kells, for patiently teaching me everything about experiments and giving me a great time working with him in lab. Thanks to Zhesi Shen for the inspiring discussions on the modelling work in Chapter 1.

I am deeply grateful to my parents for their unconditional love. For nurturing, educating, and supporting me. For letting me follow my passion. For showing me their exceptional strength and endurance. For giving me an unparalleled loving and caring family. Their love made me the richest person in the world.

Special thanks to people who helped me in my most difficult time. To my best friends, Ying Sun and Zijing Xu, for always being there for me whenever I have needed them. To friends who accompanied me, comforted me, and encouraged me. To those who brought me positivity and vitality in life. To the one who I have never met but provided me strong guidance and support. Without these people, I would not have had the faith to complete my PhD.

PUBLICATIONS

Li, J., & Shew, W. L. (2020). Tuning network dynamics from criticality to an asynchronous state. *PLOS Computational Biology*, 16(9), e1008268. *

Li, J., Kells, P. A., Gautam, S. H., & Shew, W. L. (preprint). Reduced complexity of brain and behavior due to MeCP2 disruption and excessive inhibition. *bioRxiv*. **

* Chapter 1 is partially a reprint of this paper.
** Chapter 2 is partially a reprint of this paper.
The dissertation author is the main investigator and the first author of these papers.

TABLE OF CONTENTS

1 Tuning Cortical States from Criticality to Asynchrony by Inhibitory Modulation

Abstract

According to many experimental observations, neurons in cerebral cortex tend to operate in an asynchronous regime, firing independently of each other. In contrast, many other experimental observations reveal cortical population firing dynamics that are relatively coordinated and occasionally synchronous. These discrepant observations have naturally led to competing hypotheses. A commonly hypothesized explanation of asynchronous firing is that excitatory and inhibitory synaptic inputs are precisely correlated, nearly canceling each other, sometimes referred to as 'balanced' excitation and inhibition. On the other hand, the 'criticality' hypothesis posits an explanation of the more coordinated state that also requires a certain balance of excitatory and inhibitory interactions. Both hypotheses claim the same qualitative mechanism - properly balanced excitation and inhibition. Thus, a natural question arises: how are asynchronous population dynamics and critical dynamics related, how do they differ? Here we propose an answer to this question based on investigation of a simple, network-level computational model. We show that the strength of inhibitory synapses relative to excitatory synapses can be tuned from weak to strong to generate a family of models that spans a continuum from critical dynamics to asynchronous dynamics. Our results demonstrate that the coordinated dynamics of criticality and asynchronous dynamics can be generated by the same neural system if excitatory and inhibitory synapses are tuned appropriately.

1.1 Introduction

Mounting experimental evidence supports the hypothesis that the cerebral cortex operates in a dynamical regime near criticality [1, 2, 3, 4, 5, 6, 7, 8, 9]. In the context of our work here, criticality refers to a boundary in the space of possible dynamical regimes. On one side of the boundary, population activity tends to be orderly with strong correlations among neurons. On the other side, neurons fire more independently of each other resulting in asynchronous population dynamics. At criticality, population dynamics are more diverse, rarely exhibiting synchronization that spans the network, but often showing coordinated firing among groups of neurons at small and intermediate scales [10, 11, 12]. Direct evidence that the cerebral cortex may indeed operate near such a boundary comes from experiments and models in which the balance of excitation (E) and inhibition (I) is disrupted. These studies show that one can push cortical dynamics from a dynamical regime consistent with criticality to a hyperactive synchronous regime by suppressing inhibition (GABA antagonists) or to a low-firing asynchronous state by increasing inhibition (GABA agonists) [13, 14, 15, 16, 17]. Also, critical dynamics can be pushed into a low-firing asynchronous regime by suppressing excitation (AMPA and NMDA antagonists) [15, 16, 17]. These observations support the hypothesis that the cortex may operate near criticality under normal conditions, but only if the proper balance of E and I is maintained.

However, not all observations of the cortex under 'normal conditions' exhibit the diverse multi-scale coordination that is expected near criticality. Indeed, many experimental measurements have revealed relatively asynchronous firing, particularly in vigilant and active behavioral conditions [18, 19, 20, 21, 22, 23]. The stark difference between the observations of

coordinated critical dynamics and asynchronous dynamics has traditionally fueled a debate about which is a better description of the cortex.

A prominent class of models, often referred to as 'balanced networks', offers an explanation of this more asynchronous activity. Beginning with the 'chaotic balanced state' hypothesis [24, 25], the idea is that E and I inputs to any given neuron wax and wane together, nearly canceling each other most of the time. During brief moments the E-I cancellation is imperfect and neurons can fire, contributing to an asynchronous and irregular activity. Over last two decades, numerous numerical and theoretical studies have addressed the dynamics and function of balanced networks (a few examples include [26, 27, 28, 29, 30]). Experiments supporting this possibility show the balance between excitation and inhibition based on whole cell recordings of E and I inputs [31, 32, 33, 34].

Both critical dynamics and asynchronous dynamics have been observed in awake animals and both seem to require balanced E and I. However, the difference in coordination of population activity for criticality versus asynchronous activity is stark. How can we reconcile these two types of neural activity? When should we expect to see the coordination of criticality; when should we expect to see asychronous activity?

Recent computational modeling efforts have begun to tackle these questions. They have shown several different ways that tuning one or a few simple parameters can result in a shift from asynchronous dynamics to critical dynamics or vice versa [35, 23, 36, 37]. For example, Priesemann and colleagues showed that tuning the input and an effective branching parameter (m in their terminology) can generate a family of models ranging from fully asynchronous to critical [35, 38]. Although very useful, this model was too abstract to identify specific biological mechanisms that might be responsible for changing m. Buendia

et al. studied networks of excitatory and inhibitory neurons and found that, for sufficiently sparse networks, a new regime emerges near criticality with weak flucutations around a moderate mean firing rate, reminiscent of some asynchronous activity [36]. Dahmen et al. also studied sparse networks of excitatory and inhibitory neurons, highligting how increasing the heterogeneity of synaptic strengths can change the dynamics of a system from traditional criticality (as discussed here) to a different type of critical regime at the "edge of chaos" which manifests with asynchronous dynamics [23]. Most recently, Girardi-Schappo et al. studied a more complex model of probabilistic leaky integrate and fire neurons [37], showing that Brunel's classic parameter space [39] includes a critical point that is adjacent to the 'asynchronous regular' regime and nearby the 'asynchronous irregular' regime studied by Brunel and others. (Touboul and Destexhe have pointed out that the 'synchronous irregular' state in Brunel's model is not consistent with criticality [40]). These models suggest a revision of the traditional debate; instead of asking which is a better description of cortical dynamics - criticality or asynchronous dynamics - we should acknowledge that cortex can generate both types of dynamics. Our work here builds on this premise, with the goal of exploring possible models of how a single cortical network might shift between critical dynamics and asynchronous dynamics.

We hypothesize that criticality requires a different kind of E/I balance than that needed to generate asynchronous activity. We address this possibility using a network-level model of probabilistic, binary neurons. By tuning excitatory and inhibitory synaptic strengths (keeping network structure and the input to the network fixed), we find that we can generate a family of models, spanning a continuum from criticality to the asynchronous networks. When synapses are strong and balanced, asynchronous network activity results.

When synapses are relatively weak and balanced, criticality results. Our results offer a possible explanation for the variety of experimental observations, suggesting that the cortex could shift its dynamical regime from near criticality to asynchrony and a continuum of intermediate states between these extremes, all while maintaining a certain type of balanced excitation and inhibition.

1.2 Methods

1.2.1 Network structure

We build a family of recurrent networks to model the connected neurons and study the behavior of the neural system. We construct the recurrent network with $N = 1000$ binary neurons, in which 80% neurons are excitatory and 20% neurons are inhibitory. We define $\alpha = 0.2$ as the fraction of the inhibitory neurons in the recurrent network. Interactions among neurons are described by an $N \times N$ connection matrix J. The element J_{ij} in the connection matrix represents the synapse strength from neuron j to neuron i. $J_{ij} = 0$ if the there is no connection from neuron j to neuron i. Each neuron randomly connects to other neurons with a probability $p = 0.2$. This probability is set according to connection probabilities found in experiments [41, 42]. The outgoing synapse strengths from an inhibitory neuron to its downstream neurons are drawn from a uniform distribution in $(0, -gw]$; the outgoing synapse strengths from an excitatory neuron to its downstream neurons are drawn from a uniform distribution in $(0, w]$. While other parameters are fixed, we tune the two parameters w and g to change the excitatory and inhibitory interactions. From the definitions, w represents the average synaptic strength, and g represents the relative strengths of inhibitory synapses

to excitatory synapses on average, which we name as I/E weight ratio in our work.

1.2.2 Eigenvalue spectrum

The behavior of the neural system largely depends on the properties of the neural network structure. One important property of network structure is eigenvalue spectrum of the connection matrix. We analyze eigenvalue spectrum of the networks based on random matrix theories in previous studies [43, 44, 45]. The connection matrix of neural network we construct has two important properties. Firstly, the matrix is a sparse matrix due to the low connection probability $p = 0.2$. Secondly, because all the out-going links from inhibitory neurons are negative and and all the out-going links from excitatory neurons are positive, the matrix consists of either negative columns or positive columns. Thus, the connection matrix can be written as:

$$J = [J_E \;\; J_I]\,, \tag{1.1}$$

where J_E corresponds to the sub-network containing connections from excitatory neurons and J_I corresponds to the sub-network containing connections from inhibitory neurons. According to random matrix theories, such a matrix has two real eigenvalues determined by the global synaptic strength and balance of excitation and inhibition. One of the real eigenvalues is 0; the other real eigenvalue λ_b depends on the overall excitation and inhibition in the matrix:

$$\lambda_b = \omega_E(1 - f_I) - \omega_I f_I, \tag{1.2}$$

where f_I is the fraction of inhibitory column; ω_E and ω_I are the expected summation of the elements in each excitatory column and inhibitory column, respectively. In addition, there is a group of complex eigenvalues locating in a circle centered at the origin on the complex

plane. The radius of the circular cloud of complex eigenvalues is determined by the more nuanced variances in the excitatory and inhibitory sub-networks:

$$R = \sqrt{N\left[(1-f_I)\sigma_E^2 + f_I\sigma_I^2\right]}, \tag{1.3}$$

where N is network size; f_I is the fraction of inhibitory columns; σ_E^2 and σ_I^2 are variance of the elements (including zeros) in the excitatory sub-network and inhibitory sub-network, respectively. These eigenvalue spectrum properties will be used when we analyze the eigenvalue spectrum of network models. They further reveal the dynamics properties of the models.

1.2.3 Dynamics

We apply a probabilistic dynamics on the recurrent network. The state of each neuron is either 1 or 0, corresponding to the neuron being active or quiescent, respectively. At each time step t, the probability of neuron i being active depends on two independent factors: synaptic inputs from other neurons and external inputs. Synaptic inputs from other neurons depend on the spiking of upstream neurons. In our model, the total synaptic input to neuron i from other neurons at time step t is defined as $I_i(t)$, and calculated as

$$I_i(t) = \sum_{j=1}^{N} J_{ij} s_j(t-1), \tag{1.4}$$

where $s_j(t-1)$ is the state of neuron j at time step $t-1$. Then, the probability p_i due to synaptic inputs from other neurons within the network is determined by the total synaptic input $I_i(t)$:

$$p_i(t) = \begin{cases} 1 & \text{for} \quad I_i(t) \geq 1 \\ I_i(t) & \text{for} \quad 0 \leq I_i(t) < 1 \\ 0 & \text{for} \quad I_i(t) < 0 \end{cases}. \tag{1.5}$$

The probability p_{ext} due to external inputs is set as $0.005/N$, corresponding to 1 externally-driven spike every 200 time steps over the network on average. The low rate of external input is chosen because one important property of critical dynamics is that they are self-sustainable without strong external input driving the system. Moreover, high rates of external input are known to preclude critical dynamics [3].

After we run the dynamics, we use the fraction of active neurons to represent spike rate at time t, and standard deviation of it throughout the trail to represent fluctuation in dynamics.

1.2.4 Branching function

Branching function is a theoretical tool developed in previous work as an alternative to mean field theory when theoretically analyzing population activity near criticality [46]. Mean field theory, a widely used method to study the behavior of high-dimensional systems in statistical physics, fails to characterize the dynamical properties near criticality. Previous study has shown that mean field theory does not work when the I/E weight ratio is low [29].

Branching function can be understood as the expected level of activity in the system at the next time step for a certain level of activity at the current time step. Mathematically, the definition of branching function $\Lambda(S)$ is the expected value of $S(t+1)$ divided by S for a given current level of activity $S(t) = S$:

$$\Lambda(S) = \mathrm{E}\big[S(t+1)|S(t) = S\big]/S, \tag{1.6}$$

where S is the fraction of active neurons in the network. If $\Lambda(S_0) > 1$, the system tends to have a higher level of activity $S > S_0$ at the next time step on average; If $\Lambda(S_0) < 1$,

the system tends to have a lower level of activity $S < S_0$ at the next time step on average. $\Lambda(S_0) = 1$ means the level of activity tends to stay at the current level S_0 on average. It may either increase or decrease due to noise or external input. Numerically, we obtain the branching function by running the model one time step forward many times for each possible level of activity. For a certain level of activity S_0, we set $S(1) = S_0$ and run the the model one time step forward to obtain $S(2)$ many times, and calculate the average $S(2)/S(1)$ as the branching function $\Lambda(S_0)$ in simulation.

1.2.5 Neural avalanche

Neural avalanche is a way to validate whether a system operates near criticality. An expectation of a system operating at criticality is that distributions of neuronal avalanche durations and sizes are power-law distributions [47, 48, 13]. Similar to previous work [15, 49, 46, 13], a neural avalanche is defined as a period of time when the number of active neurons exceeds a threshold, as shown in Fig. 1.4a. Then, the duration and size of an avalanche are defined as the number of time steps and the number of spikes during the avalanche, respectively. The threshold of the activity level for avalanches is selected based on branching function as in previous work [46]. Specifically, we set the threshold at level $S^\dagger$ when the branching function $\Lambda(S^\dagger) = 1.01$ in our work.

We run the dynamics long enough to get a large number of neural avalanches in order to examine the distributions of neuronal avalanche durations and sizes. After obtaining distributions, we calculate a measurement κ_ϵ to examine if the distributions are close to

power-law distributions with exponent $-\epsilon$ as in previous work [16]. κ_ϵ is defined as

$$\kappa_\epsilon = 1 + \frac{1}{10}\sum_{i=1}^{10} F_\epsilon^{\mathrm{NA}}(\beta_i) - F(\beta_i), \tag{1.7}$$

where F is the cumulative distribution function of the examined avalanche duration or size, while F_ϵ^{NA} is the cumulative distribution function of the reference power-law distribution with exponent $-\epsilon$. β_i is the ith representative sample taken into calculation in the cumulative distribution function. We take 10 logarithmically spaced points as representative samples along the measured distribution in our work. From the definition of κ_ϵ, if the examined distribution is close to the reference power-law distribution, κ_ϵ is close to 1. In contrast, κ_ϵ deviates form 1 if the examined distribution does not match the reference power-law distribution well. $\kappa_\epsilon > 1$ means the examined distribution has more large avalanches than the reference power-law distribution; $\kappa_\epsilon < 1$ means the examined distribution has fewer large avalanches than the reference power-law distribution.

1.2.6 Synaptic input

To examine how the balance of excitation and inhibition is reflected in synaptic current at the single cell level, we calculated the total synaptic input, excitatory synaptic input, and inhibitory synaptic input for each neuron. The total synaptic input $I_i(t)$ to neuron i at time step t is separated into excitatory synaptic input $I_i^{\mathrm{E}}(t)$ and inhibitory synaptic input $I_i^{\mathrm{I}}(t)$ by counting only positive connections (when $J_{ij} > 0$) or negative connections (when $J_{ij} < 0$), respectively. When excitatory synaptic current and inhibitory synaptic current are tightly balanced, $I_i^{\mathrm{E}}(t)$ and $I_i^{\mathrm{I}}(t)$ cancel each other and the total synaptic input $I_i(t)$ is close to 0. We define an E/I tension T_i to measure how tightly the $I_i^{\mathrm{E}}(t)$ and $I_i^{\mathrm{I}}(t)$ are balanced

for neuron i:

$$T_i = 1 - \frac{\langle I_i(t) \rangle}{\langle I_i^{\mathrm{E}}(t) \rangle + \langle |I_i^{\mathrm{I}}(t)| \rangle}, \tag{1.8}$$

where $\langle \cdot \rangle$ represents time average. From the definition, T_i is close to 1 if $I_i^{\mathrm{E}}(t)$ and $I_i^{\mathrm{I}}(t)$ are tightly balanced for neuron i. Then, we use the average of T_i over all neurons to obtain the E/I tension T of the network.

1.2.7 Cross-correlogram

Whether the neurons are weakly or strongly correlated across network and time is an important property of the population activity. To examine this property, we look at the population-averaged cross-correlogram (CCG) of synaptic inputs. We plot the CCGs by calculating the cross correlations of synaptic inputs across neurons with time lags from -20 to 20 time steps. The larger the area under the CCG curve is, the stronger the neurons are correlated across time; in contrast, the smaller the area under the CCG curve is, the weaker the neurons are correlated across time.

CCGs are especially used for testing an essential property of asynchronous dynamics: there is weak correlations of synaptic input across neurons and time. Previous work has shown that the weak correlation of total synaptic input comes from the closely traced and canceled excitatory and inhibitory synaptic input [19]. Thus, in addition to total synaptic input (Total-Total), we also examine CCGs of excitatory synaptic inputs (E-E), inhibitory synaptic inputs (I-I), and excitatory and inhibitory synaptic inputs (E-I, I-E). Based on the areas under the CCG curves, we define a desynchronization η to measure how much the asynchrony of the total synaptic input is caused by the cancellation of the synchronized

excitatory and inhibitory synaptic inputs:

$$\eta = 1 - \frac{A_{\text{Total}}}{(A_{\text{EE}} + A_{\text{II}})/2}, \tag{1.9}$$

where A_{Total} is the area under CCG of total synaptic input, and A_{EE} and A_{II} are the area under CCGs of excitatory and inhibitory synaptic, respectively.

1.2.8 Inter-spike intervals

The inter-spike interval (ISI) is another important feature of population activity. The coefficient of variation (CV) of inter-spike intervals is larger when the population activity is more bursty. Especially, asynchronous dynamics is often associated with Poisson firing, where the CV of ISI is near 1. We calculate the distributions of ISIs in our models, as well as CV of ISI, to examine if the population activity is close to Poisson firing.

1.3 Results

We study the recurrent networks described in Methods varying two parameters: the average synaptic weight and the relative strengths of inhibitory and excitatory synapses (the I/E weight ratio). Thus, there is a family of models on the two-dimensional parameter space. We first look at behavior of the dynamics, including firing rate and fluctuations. Then, we theoretically analyze the eigenvalue spectrum of the networks and branching function of dynamics to explain the behavior of the family of models. Next, we examine dynamic properties regarding criticality in the family of models. Last, we examine dynamic properties regarding asynchronous activity in the family of models.

1.3.1 Behavior of the network dynamics

We first consider how the average spike rate and its standard deviation depend on the two parameters, as shown in Fig. 1.1a, b. Through simulation, we find that a majority of the top-left area in the two-dimensional parameter space is occupied by a high spike rate with low standard deviation, dominated by excitation. In contrast, a majority of the bottom-right area is occupied by a low spike rate with low standard deviation, dominated by inhibition. In these two areas, the dynamics either saturate or die out with no fluctuation, and thus are not realistic models for cortical network dynamics. The boundary between these two areas, however, has moderate spike rate and standard deviation, i.e. reasonable level of activity and fluctuation. Along this boundary, neither excitation nor inhibition dominates, and the dynamics are realistic models for cortical network dynamics.

We are particularly interested in the dynamics along the boundary where realistic cortical dynamics occur. To identify this boundary more precisely, we look at the largest eigenvalue of the connection matrix for the models (Fig. 1.1c). In the high spike rate region (top-left), the largest eigenvalue is greater than 1; In the high spike rate region (bottom-right), the largest eigenvalue is smaller than 1. The largest eigenvalue along the boundary, however, is near 1. Having the largest eigenvalue near 1 indicates that the dynamics do not systematically grow nor decay as time passes, which reasonably models real brain activity. We indicate models having the largest eigenvalue equal to 1 with green line in Fig 1.1a-c. The line closely fits the boundary when the I/E weight ratio is low (bottom-left). Small deviation from the line leads to saturating or dying-out dynamics in this regime. The setting of parameters in this regime are similar to models used in previous studies of criticality

[50, 51, 15], where parameters are set such that the largest eigenvalue equals to 1. As the I/E weight ratio increases along the boundary, the dynamics deviate from criticality. A larger region in the parameter space results in a sustainable dynamics without saturating or dying-out (top-right). In this regime, the dynamics are sustained through another mechanism. Since the line of having the largest eigenvalue equal to 1 always lies in the boundary between the high spike rate and low spike rate regions, and well represents different regimes for reasonable dynamics modeling brain activity, we study the dynamics along this line in more detail.

We first look at the average spike rate and its standard deviation along the line of having the largest eigenvalue equal to 1 (Fig. 1.1d, e). The spike rate and its standard deviation vary along the line, but always fall in a reasonable range. Counterintuitively, as the I/E weight ratio increases from 0 to around 3, the average spike rate increases along with a higher inhibition. However, this is consistent with previous study that inducing inhibition helps to maintain the dynamics sustainable [46]. As I/E weight ratio further increases from around 3 to beyond 4, the average spike rate decreases to a lower level. The standard deviation of spike rate, i.e. fluctuation in the dynamics, increases as I/E weight ratio increases from 0, and reaches the peak when I/E weight ratio is around 1. After I/E weight ratio goes beyond 1, the standard deviation gradually decreases to a low level.

We wonder how the excitatory and inhibitory synaptic strengths change as functions of the I/E weight ratio to keep the largest eigenvalue equal to 1. As shown in Fig. 1.1f, the change of synaptic strengths is not linear. Excitatory synaptic strength increases to counter-balance the larger inhibitory synaptic strength as I/E weight ratio goes up. Therefore, at the bottom-left regime in the two-dimensional parameter space, it is when the weak excitation

is balanced by a weak inhibition; at the top-right regime in the two-dimensional parameter space, it is when the strong excitation is balanced by a stronger inhibition. These two different types of balance between excitation and inhibition generate very different dynamics.

We find the behavior of dynamics varies dramatically along the boundary with different types of balance between excitation and inhibition. We take two examples on the line of having the largest eigenvalue equal to 1 ($\lambda_{max} = 1$): at the blue triangle and pink triangle in Fig. 1.1a-c. For weak synapses and smaller I/E ratios (near the blue triangle in Fig. 1.1a-c), the $\lambda_{max} = 1$ boundary is sharply defined. Population activity is synchronous and coordinated fluctuations are large. Fig. 1.1g shows the raster plot of the dynamics at the blue triangle in the two-dimensional parameter space. It is noteworthy that our model operates at criticality when $\lambda_{max} = 1$ and I/E = 0 according to previous study [52]. In contrast, for stronger synapses and higher I/E ratios, the boundary is less sharply defined (near the pink triangle in Fig. 1.1a-c). Population activity is asynchronous and fluctuations are less prominent. Fig. 1.1h shows the raster plot of the dynamics at the pink triangle in the two-dimensional parameter space. The eigenvalue spectra of the connectivity matrix for weak-synapse regime and the strong-synapse regime also differ qualitatively. The eigenvalue spectrum in the weak-synapse and low I/E regime is dominated by a single outlying eigenvalue 1 (Fig. 1.1i). The eigenvalue spectrum in the strong-synapse and high I/E regime, however, consists of cloud of eigenvalues in the complex plane with radius 1 centered at the origin, without any dominant eigenvalue (Fig. 1.1j).

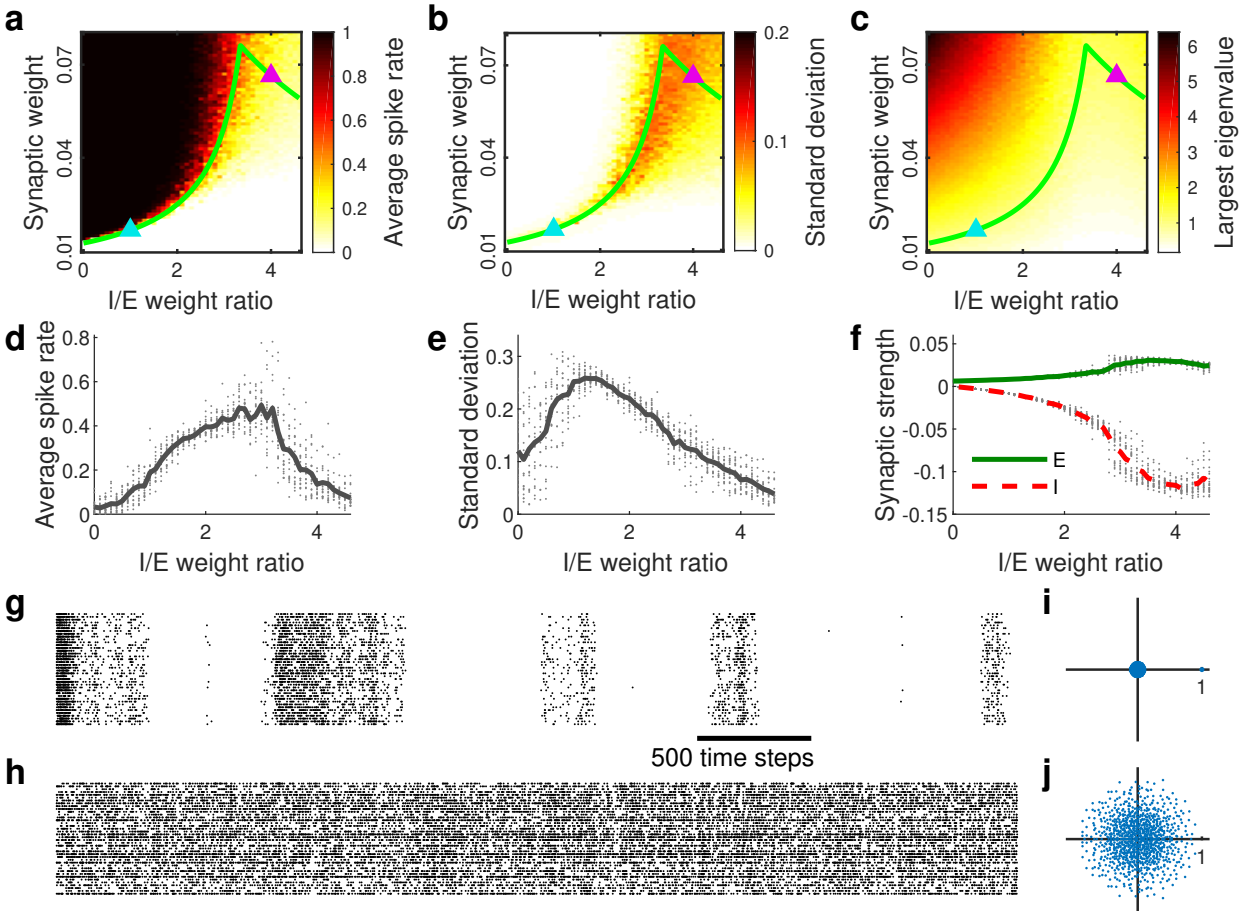

Figure 1.1: Synchronous and asynchronous dynamical regimes along the $\lambda_{max} = 1$ boundary. (a) Time averaged population spike rate as a function of I/E weight ratio and synaptic weight. The $\lambda_{max} = 1$ boundary (green line) divides a high firing rate regime (black) from a low firing rate regime (white). (b) Standard deviation of the population spike rate across time as a function of I/E weight ratio and synaptic weight. Fluctuations are largest along the $\lambda_{max} = 1$ boundary. (c) The largest eigenvalue λ_{max} of the synaptic weight matrix as a function of I/E weight ratio and synaptic weight. $\lambda_{max} > 1$ in the high firing rate regime and $\lambda_{max} < 1$ in the low rate regime. (d) Shown is the spike rate along the $\lambda_{max} = 1$ boundary. The spike rate is moderate all along the boundary. (e) Shown is the amplitude of spike rate fluctuations (standard deviation across time) along the $\lambda_{max} = 1$ boundary. (f) Excitatory and inhibitory synaptic weights balance each other but become stronger as I/E weight ratio is increased along the $\lambda_{max} = 1$ boundary. (g,h) Example spike rasters for the low and high I/E ratio regimes, corresponding to the blue and pink triangles in panels a-c, respectively. (i,j) Eigenvalue spectra for the two examples in panels g and h.

1.3.2 Theoretical analysis

To better understand how the models show dramatically different behaviors, we theoretically analyze eigenvalue spectrum of the networks and branching function of the dynamics, as described in Methods.

Eigenvalue spectrum

The connectivity matrix in our models has two real eigenvalues and a group of complex eigenvalues according to random matrix theories in previous studies [43, 44, 45]. The two real eigenvalues are determined by the global synaptic strength and balance of excitation and inhibition. One is 0 and the other one is determined by Eq. 1.2 in Methods:

$$\lambda_b = \omega_E(1 - f_I) - \omega_I f_I.$$

Specifically in our models, the fraction of inhibitory columns is $f_I = \alpha$; the expected summation of the elements in an excitatory column is $\omega_E = Npw/2$; the expected summation of the the elements in a inhibitory column is $\omega_I = Npgw/2$. Thus, the magnitude of the non-trivial real eigenvalue is

$$\lambda_b = \frac{w}{2}Np(1 - \alpha) - \frac{gw}{2}Np\alpha. \tag{1.10}$$

On the other hand, the group of complex eigenvalues are related to the substructure of excitation and inhibition in the matrix. They consist a circular cloud centered at the origin on the complex plane. The radius of the cloud is determined by Eq. 1.3 in Methods:

$$R = \sqrt{N\left[(1 - f_I)\sigma_E^2 + f_I\sigma_I^2\right]}.$$

Again, the fraction of inhibitory columns is $f_I = \alpha$ in our models. The variance of all the elements in the excitatory sub-network σ_E^2 and inhibitory sub-network σ_I^2 can be derived as follows. For the excitatory sub-network, there are $Np(1-\alpha)$ positive numbers uniformly distributed in $[0, w]$ and $N(1-p)(1-\alpha)$ zeros. Thus, the variance of the excitatory sub-network is

$$\begin{aligned}
\sigma_E^2 &= EX^2 - (EX)^2 \\
&= p\left(\frac{1}{w}\int_0^w x^2 dx\right) - \left[p\left(\frac{w}{2}\right)\right]^2 \\
&= \frac{p}{3}w^2 - \frac{p^2}{4}w^2 \\
&= \left(\frac{p}{3} - \frac{p^2}{4}\right)w^2.
\end{aligned} \tag{1.11}$$

Similarly, the variance of the inhibitory sub-network is

$$\sigma_I^2 = \left(\frac{p}{3} - \frac{p^2}{4}\right)(gw)^2. \tag{1.12}$$

Therefore, the radius of the cloud of complex eigenvalues is

$$R = \sqrt{N\left[(1-\alpha)\sigma_E^2 + \alpha\sigma_I^2\right]}\,, \tag{1.13}$$

where σ_E^2 and σ_I^2 are expressed in Eq. 1.11 and Eq. 1.12, respectively.

Taken together, the largest eigenvalue of the connectivity matrix of the models is the larger one of the real non-trivial eigenvalue λ_b and the radius of the complex eigenvalue cloud R:

$$\lambda_{max} = \max\left(\lambda_b, R\right). \tag{1.14}$$

Whether λ_b or R is larger determines the behavior of dynamics. Having a dominating largest eigenvalue at 1, i.e. $\lambda_b = 1$ and is markedly larger than R, is a condition of the system operating at criticality. In this scenario, the dynamics are relatively coordinated and

synchronous as seen in Fig. 1.1g. In contrast, when there is not a dominating eigenvalue, the dynamics are influenced by more eigenvalues, which results in a high-frequency fluctuation and asynchronous dynamics as seen in Fig. 1.1h.

We next seek to quantitatively determine when the models fall into which scenario. Setting $\lambda_b = R$, we have

$$\frac{w}{2}Np(1-\alpha) - \frac{gw}{2}Np\alpha = \sqrt{N\left[(1-\alpha)\left(\frac{p}{3}-\frac{p^2}{4}\right)w^2 + \alpha\left(\frac{p}{3}-\frac{p^2}{4}\right)(gw)^2\right]}\,. \tag{1.15}$$

We find that after w cancels out on each side, the only varying parameter left in the equation is the I/E weight ratio g. Thus, whether λ_b or R is larger depends only on the I/E weight ratio g, and is independent of the synaptic strength w. We further rearrange the equation to find the switching point g^*:

$$g^* = \frac{p(1-\alpha)\alpha + \sqrt{p^2(1-\alpha)^2\alpha^2 - \left[p\alpha^2 - \left(\frac{4}{3}-p\right)\alpha/N\right]\left[p(1-\alpha)^2 - \left(\frac{4}{3}-p\right)(1-\alpha)/N\right]}}{p\alpha^2 - \left(\frac{4}{3}-p\right)\alpha/N}. \tag{1.16}$$

With the parameters set in our model ($N = 1000$, $p = 0.2$, and $\alpha = 0.2$), the switching point is at $g^* = 3.34$. This explains the turning point on the line of having the largest eigenvalue equal to 1 in Fig. 1.1a-c. It is noteworthy that this turning point is under the condition of a limited network size. At large limit N, we have

$$g^* = \frac{p(1-\alpha)\alpha}{p\alpha^2} = (1-\alpha)/\alpha. \tag{1.17}$$

With the widely used fraction of inhibitory neurons $\alpha = 0.2$, we have $g^* = 4$.

We validate that the theoretical analysis of eigenvalue spectrum well explains the largest eigenvalue in simulations. Fig. 1.2 shows the largest eigenvalue calculated theoretically, which highly agrees with the largest eigenvalue obtained from simulations (Fig. 1.1c).

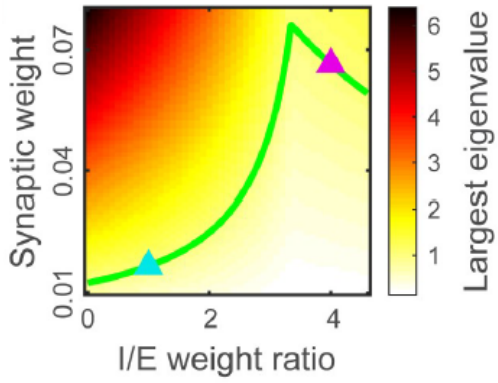

Figure 1.2: The theoretical largest eigenvalue of the synaptic weight matrix as a function of I/E weight ratio and synaptic weight derived in Sec. 1.3.2. Green line indicates the line of $\lambda_{max} = 1$. Blue and pink triangles indicates the dynamics corresponding to the spiking rasters in Fig. 1.1g and Fig. 1.1h, and eigenvalue spectra in Fig. 1.1i and Fig. 1.1j, respectively.

Branching function

We next use branching function as a theoretical tool to analyze the average spike rate and fluctuation of the dynamics. The branching function was developed in previous work to theoretically analyze population activity near criticality [46]. This approach is an alternative to using mean field theory, which fails to characterize the dynamical properties when the I/E weight ratio is low [29]. First, we define $S(t)$ as the fraction of neurons in the network that are firing at time t. Then, the branching function $\Lambda(S)$ is defined as the expected value of $S(t+1)/S(t)$ conditioned on the level of activity $S(t)$, as defined in Eq. 1.6 in Methods:

$$\Lambda(S) = \mathrm{E}\big[S(t+1)|S(t) = S\big]/S.$$

By combining the definition of branching function and the dynamics in our models, we obtain a prediction for the branching function:

$$\Lambda(S) = \frac{1}{S} E\left[\sigma\left(\sum_{i=1}^{n_E} J_{E_i} - \sum_{j=1}^{n_I} J_{I_j}\right)\right], \tag{1.18}$$

where n_E and n_I are the number of active presynaptic excitatory and inhibitory neurons, respectively. Here, σ is the step-wise linear function with the same form as the firing probability due to synaptic inputs, $p_i = \sigma(I_i(t))$, in Eq. 1.5. J_{E_i} and J_{I_j} represent the ith excitatory and jth inhibitory synaptic strength, respectively. Considering the synaptic strength on average, we have

$$\begin{aligned}\Lambda(S) &= \frac{1}{S} E\left[\sigma\left(\frac{w}{2} n_E - \frac{gw}{2} n_I\right)\right] \\ &= \frac{1}{S} \sum_{n_E=1}^{N} \sum_{n_I=1}^{N} P(n_E) P(n_I) \sigma\left(\frac{w}{2} n_E - \frac{gw}{2} n_I\right),\end{aligned} \tag{1.19}$$

where $P(n_E)$ and $P(n_I)$ are probabilities of having the number of active presynaptic excitatory and inhibitory neurons equal to n_E and n_I, respectively. We further assume n_E and n_I are Poisson variables with means $\mu_E = Np(1-\alpha)S$ and $\mu_I = Np\alpha S$ to have specific forms of $P(n_E)$ and $P(n_I)$. With this semi-analytical method, we obtain a good prediction for $\Lambda(S)$ (solid lines in Fig 1.3a) compared to simulations (dash lines in Fig 1.3a).

The shape of branching function reveals the properties of dynamics. We find two distinct shape of branching functions in the weak-synapse and strong-synapse regimes. In the weak-synapse, the synchronous regime, the branching functions have a wide range near $\Lambda(S) = 1$ (blue line in Fig 1.3a). Since $\Lambda(S) = 1$ means the level of population activity does not systematically grow or decay in the next time step, the 'flat' branching function indicates that the system is able to wander through various population firing rates. This has been considered as a hallmark of criticality in previous work [46]. In this regime, the population activity often fluctuates greatly around the mean, as expected due to a wide range near $\Lambda(S) = 1$ in the branching function. In contrast, in the strong-synapse, the asynchronous regime, the branching function has a substantial slope, crossing $\Lambda(S^*) = 1$ at a particular

value of $S = S^*$ (pink line in Fig 1.3a). In this scenario, the firing rate is relatively stable with small fluctuations around $S = S^*$.

We use the shape of branching function to predict the properties of dynamics in the two-dimensional parameter space. We first use the semi-analytical method described above to determine the shape of the branching function. Then, we use the crossing point of $\Lambda(S^*) = 1$ to predict the average spike rates as S^*. We are able to obtain good qualitative predictions (Fig 1.3b) of the average spike rates that we observe when we run our model (Fig 1.1a). To predict the fluctuations in the dynamics, we define a 'critical range' ρ to measure the range of the branching function that stays within a certain distance of 1. Critical range is defined as $\rho = S_2 - S_1$, where S_1 and S_2 are the fractions of active nodes when $\Lambda(S_1) = 1.05$ and $\Lambda(S_2) = 0.95$, as shown in Fig 1.3a insert. The large critical range in the synchronous regime (Fig 1.3c) fits reasonably well with the large standard deviation in simulations (Fig 1.1b). The weak-synapse regime has large critical range, while the strong-synapse regime has small critical range.

In conclusion, both simulation and theoretical analysis indicate that along the line of having the largest eigenvalue equal to 1 ($\lambda_{max} = 1$), the dynamics in low I/E and weak-synapse regime operate at criticality, while the dynamics in high I/E and strong-synapse regime are asynchronous dynamics. In the remainder of this chapter, we examine differences between these two regimes: the synchronous regime at a low I/E weight ratio and weak synaptic strength, and the asynchronous regime at a high I/E weight ratio and strong synaptic strength. We examine properties of dynamics traditionally associated with criticality including neuronal avalanche size and duration distributions [46, 13, 47]. We also examine several aspects of dynamics related to asynchronous neural dynamics including cancellation

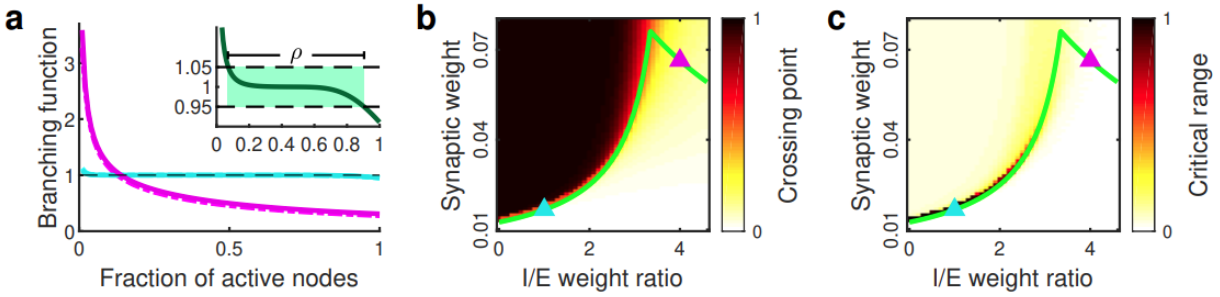

Figure 1.3: Analysis of branching functions explains model behavior. (a) Branching functions Λ are distinctly different for networks in the synchronous regime (blue) and asynchronous regime (pink). Solid lines are calculated semi-analytically and dash lines are obtained from simulating the model. Inset: The critical range ρ is defined as the range of S for which $\Lambda(S)$ lies between 1.05 and 0.95. (b) Crossing point where $\Lambda = 1$ as a function of I/E weight ratio and synaptic weight, which successfully reproduces average spike rate in simulations. (c) Critical range as a function of I/E weight ratio and synaptic weight.

of E and I inputs, correlation functions, and inter-spike intervals [19, 26, 31]. In agreement with previous work, we will show that the weak-synapse $\lambda_{max} = 1$ boundary corresponds with criticality, while strong synapses and $\lambda_{max} = 1$ result in asynchronous dynamics.

1.3.3 Properties related to criticality

We examine the distributions of neuronal avalanche sizes and durations along the boundary of $\lambda_{max} = 1$ (green line in Fig 1.1 and Fig 1.3). An important expectation near criticality is that distributions of neuronal avalanche sizes and durations should have power-law form [47, 48, 13]. Similar to previous work [49, 46, 13], we define an avalanche as a period of time during which the number of active neurons exceed a threshold, as shown in Fig 1.4a. The duration and size of an avalanche are defined as the number of time steps and the total number of spikes that occurred during the avalanche, respectively. We find that both avalanche duration and size distributions change dramatically along the line of

having $\lambda_{max} = 1$ (Fig 1.4b). When the I/E weight ratio is low, the avalanche duration and size distributions are close to power-law distributions (blue lines in Fig 1.4b), as expected at criticality. As the I/E weight ratio increases, the distributions of avalanche duration and size deviate from power-law distributions (green, yellow, orange, and red lines in Fig 1.4b), with large avalanches becoming less prominent.

We use κ_ϵ to quantify how much a distribution deviates from a power-law distribution with exponent $-\epsilon$ as described in Methods, which origins from previously studies [15, 5, 13, 49]. If the distribution is close to the power-law distribution, κ_ϵ is close to 1, which occurs for both avalanche duration and size distributions when the I/E weight ratio is low. We consider $\epsilon = 1.5$ for the size distributions and $\epsilon = 1.7$ for the duration distributions, which are the best-fitted exponents with $g = 0$ and $\lambda_{max} = 1$. Moreover, 1.5 has been widely observed as the exponent for avalanche sizes at criticality [47, 53, 54]. Any deviation in κ_ϵ from 1 means a deviation from the power-law distribution. As the I/E weight ratio grows larger, κ_ϵ starts to deviate from 1, then varies erratically for intermediate I/E before settling near $\kappa_\epsilon = 0.8$ as I/E approaches 4. Since power-law avalanche size and duration distributions are a necessary condition for criticality, we conclude that our model deviates from criticality as the I/E weight ratio is increased along the $\lambda_{max} = 1$ boundary. This is consistent with previous work with similar models [50, 51, 15].

1.3.4 Properties related to asynchronous activity

We study properties predicted by some theories to occur in asynchronous neural activity. We first examine the excitatory and inhibitory inputs to the model cells. For all I/E ratios, E and I inputs are strongly correlated, but as we increase the I/E ratio,

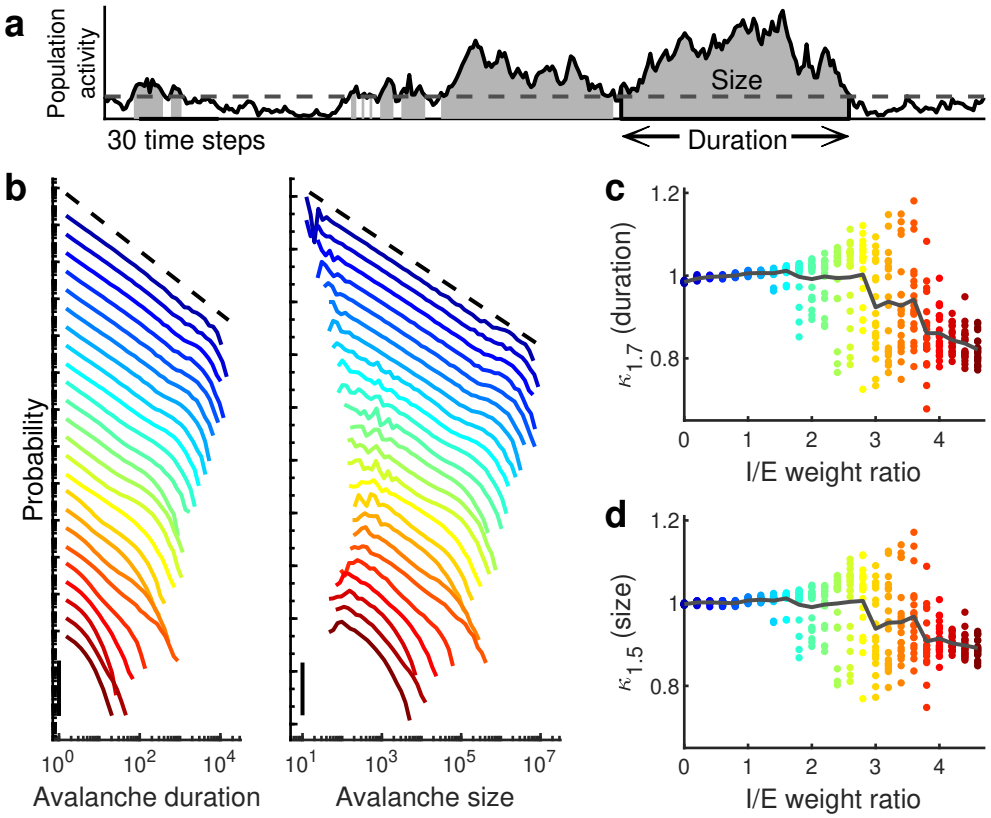

Figure 1.4: Avalanche distributions indicate deviation from criticality as I/E ratio is increased. (a) An avalanche is defined as a time period during which the number of active neurons (solid line) exceeds a threshold (dashed line). Avalanche duration is the number of time steps included in an avalanche, while avalanche size is the number of spikes included in an avalanche. (b) The probability distributions of avalanche duration and size for different I/E weight ratios. Color represents different I/E weight ratios as in panels c and d. Vertical axis is logarithmic with the scale bar showing 3 orders of magnitude. Distributions are shifted vertically for comparison. (c) Deviation from a power law with exponent -1.7 is measured by $\kappa_{1.7}$ for avalanche duration as a function of I/E weight ratio. (d) Deviation from a power law with exponent -1.5 is measured by $\kappa_{1.5}$ for avalanche size as a function of I/E weight ratio. For each I/E, we generate multiple realizations (dots) and average them to obtain the mean (solid line).

the dynamics are tuned from a state in which excitatory input dominates (is not canceled by inhibition) to a state in which inhibitory input cancels the excitatory input more and more exactly (Fig 1.5a-c). We define 'E/I tension' to measure how tightly the excitatory and inhibitory inputs cancel each other (Methods). Fig 1.5d shows that the E/I tension gradually increases as the I/E weight ratio increases, and reaches as high as 1 when the I/E weight ratio is 4. This result is consistent with previous work showing that tightly balanced E and I currents canceling each other leads to asynchrony [26].

Another essential property of asynchronous population activity is that neurons should be weakly correlated across neurons and across time. Thus, we next examine the population-averaged input cross-correlogram (CCG) for different I/E weight ratios (Fig 1.5e-g). When the I/E weight ratio is low, CCGs of excitatory, inhibitory and total inputs all reveal strong correlations across neurons and over long timescales. As the I/E weight ratio increases, CCGs decrease in amplitude and timescale. When the I/E weight ratio is high, although the excitatory and inhibitory input CCGs remain relatively high at zero delay, the total input CCG is weak due to balance between excitatory and inhibitory inputs. We quantify asynchrony based on decreases in temporal and cross-neuron correlations. For this, we define η to be inversely proportional to the area under CCG for total input (normalized as defined in the Methods). As shown in Fig 1.5h, asynchrony η sharply increases when the I/E weight ratio goes beyond 2, and reaches a high value when the I/E weight ratio is over 3, consistent with the turning point in the eigenvalue analysis. Therefore, strong inhibition makes excitatory and inhibitory inputs balanced and leads to asynchronous activity. This is in accordance with the result in previous work that the population-averaged firing correlation is weak when inhibition is strong and fast [19]. Considering together the balance of E and I inputs and the

asynchronous firing, we conclude that high I/E with strong synaptic strength in our model is consistent with two prominent expectations for asynchronous network activity.

Finally, we consider the coefficient of variation (CV) of inter-spike-intervals (ISI). For Poisson firing, which is often associated with asynchronous dynamics, the CV of ISI is near 1, while more bursty firing will have CV of ISI greater than 1. We find that in the weak-synapse, synchronous regime, ISI distributions are similar across neurons, while in the strong-synapse, asynchronous regime, ISI distributions are more varied across neurons (Fig 1.5i-k). Moreover, as I/E weight ratio is increased, the CV of ISI (averaged across neurons) is high for low I/E ratios, decreasing to near 1 in the asynchronous regime (Fig 1.5l).

1.4 Discussion

We have shown that the population activity of neural networks can vary dramatically depending how excitation and inhibition are balanced. If weak excitation is balanced by weak inhibition, we found that the dynamics exhibit large fluctuations and rather coordinated activity at criticality. If stronger inhibition balances stronger excitation in a higher "tension" balance, we found that the dynamics are asynchronous and steady. Along with other recent studies [35, 36, 23, 37], our findings suggest that the same cortical network could be tuned from criticality to asynchrony, by tuning inhibition and excitation appropriately.

How do our results compare to other recent studies relating critical dynamics to asynchronous dynamics? In the work of Priesemann and colleagues, they found that critical dynamics can shift toward asynchronous dynamics when they reduced the efficacy of activity propagation (their m parameter), while increasing the input to the network [35, 38]. They have also shown how homeostatic plasticity mechanisms can act to give rise to a range of

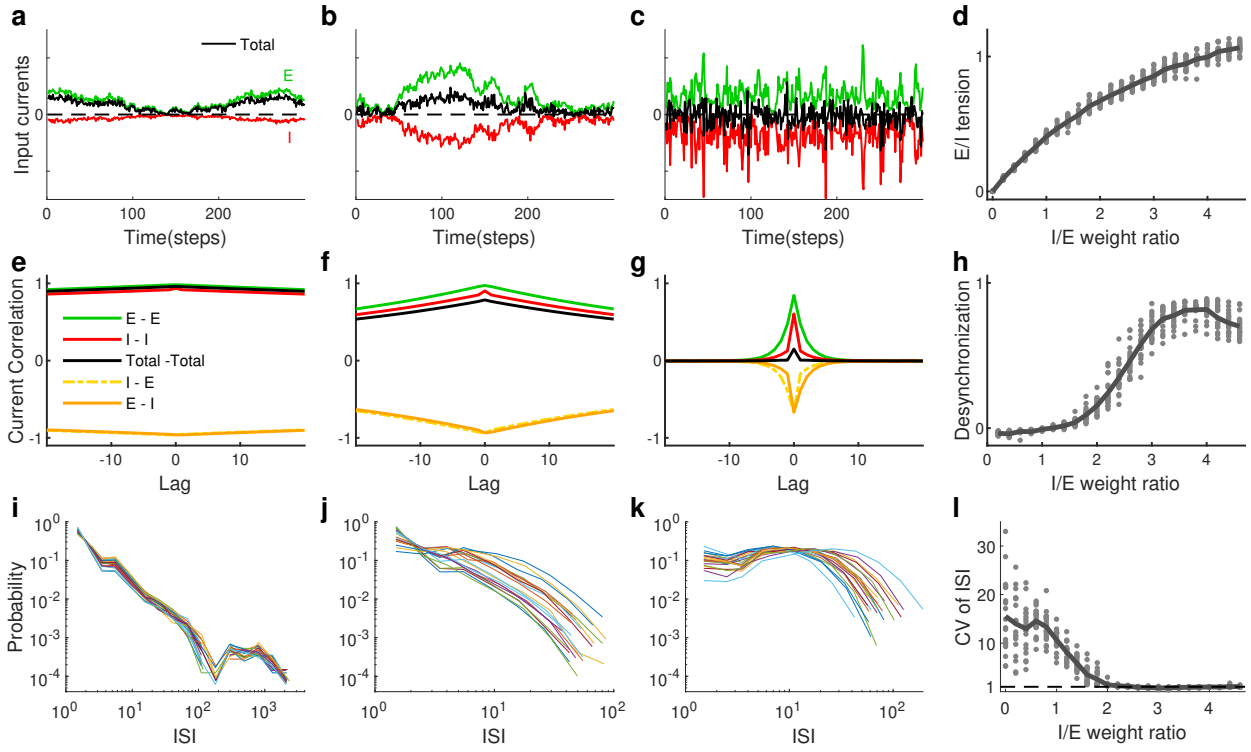

Figure 1.5: Excitatory inputs cancel inhibitory inputs in asynchronous regime for high I/E. (a-c) Synaptic inputs when the I/E weight ratios are 1, 2 and 4, respectively. The excitatory (green) and inhibitory (red) inputs are shown separately from the total synaptic input (black). (d) E/I tension as a function of the I/E weight ratio. For each I/E, we generate multiple realizations (dots) and average them to obtain the mean (solid line). (e-g) Population-averaged cross correlograms (CCGs) of total synaptic inputs (black), excitatory inputs (green) and inhibitory inputs (red) when the I/E weight ratios are 1, 2 and 4, respectively. (h) The level of desychronization η as a function of I/E weight ratio. For each I/E, we generate multiple realizations (dots) and average them to obtain the mean (solid line). (i-k) Distributions of inter-spike-intervals (ISI) are similar across neurons for the low I/E regime, more varied across neurons for the high I/E regime. (l) The coefficient of variation (CV) of ISI as a function of the I/E weight ratio. CV of ISI is high for small I/E and approaches 1 as the I/E weight ratio is increased. For each I/E, we generate multiple realizations (dots) and average them to obtain the mean (solid line).

dynamical regimes including criticality and asynchronous states, depending on the input to the system [55]. In contrast, in our model, we kept input to the network fixed while strengthening synapses to tune the network from criticality to asynchrony. Since stronger synapses are more effective for propagating activity, we suspect our work points to a different mechanism than that discussed by Priesemann and colleagues. Buendia et al. focused on the 'low-activity intermediate' (LAI) regime, which had small fluctuations similar asynchronous regimes [36]. Their LAI regime emerged when they reduced the density of connections to a sufficiently sparse level (less than 0.01). In our model the density of connections was 0.2, which suggests that our model is dealing with a different type of asynchronous regime. Our observed changes in eigenvalue spectra as we tuned our model from criticality to asynchrony are similar to those studied by Dahmen et al. when they compared two types of critical dynamics [23]. As the outlying real eigenvalue comes closer to the bulk of complex eigenvalues, while maintaining a largest eigenvalue near 1, traditional criticality (like that discussed here) is replaced with "edge of chaos" criticality. Like our case, this change in eigenvalues and dynamics was also accompanied by changes in the relative strengths of excitatory and inhibitory synapses in their model. These similarities suggest that the asynchronous regime in our model might correspond to "edge of chaos" criticality, but, considering the differences in their model (firing rate) and ours (probabilistic binary neurons), a more careful study would be required to test this possibility. Finally, we note that Girardi-Schappo et al. found that a network of probabilistic leaky-and-fire neurons can be tuned from criticality to an 'asynchronous irregular' regime (as defined by [39]) by strengthening inhibition relative to excitation (increasing their g parameter) [37]. Our model, considered together with the work of Girardo-Schappo et al. and Dahmen et al. suggests that there may be a

general principle governing our models; perhaps increasing the strength of inhibition relative to excitation, while maintaining balance, will always result in a shift away from criticality, towards asynchronous dynamics. Additional theoretical work will be required to test this possibility.

In our work here, our goal was to start with a model that is well-understood to operate at criticality and then push that model away from criticality to generate asynchronous dynamics. Other studies have approached a similar question starting from models with well-understood asynchronous dynamics and pushing them into regimes with larger population-level fluctuations (but not criticality). For example, Ostojic found that the asynchronous balanced state can become unstable with large population-level fluctuations (termed the 'heterogeneous asynchronous state') [29]. They implemented this change by increasing synaptic strengths, starting with $\lambda_{max} < 1$ and resulting with $\lambda_{max} > 1$. Other recent studies have extended asynchronous balanced networks to regimes with coherent activities [30, 56]. However, none of these studies approached the critical regime.

One interesting hypothesis that emerges from our work concerns metabolic efficiency. First, we note that maintaining a "strong" synapse depends on metabolically expensive biophysical mechanisms - greater presynaptic vesicle pool, greater density of postsynaptic receptors, etc. Since the high I/E regime and the low I/E regime have similar mean firing rates, it stands to reason that the strong synapses of the high I/E scenario would consume more metabolic resources than the lower I/E scenario. Moreover, the critical dynamics we observed at low I/E are associated with a number of functional benefits [12, 4, 13]. On the other hand, the lower fluctuations found in the high I/E regime may be beneficial for functions that require lower "noise" [26, 24, 4]. When low noise is not required, perhaps the

brain could tune itself to the low I/E regime where energy consumption is less. This is consistent with the observation that resting, awake animals tend to exhibit greater fluctuations in population activity compared to alert, active animals. Experimental tests of this idea would be challenging, requiring comparisons of synaptic strengths across behavioral states. We would predict that alert, active states would exhibit stronger synapses (i.e. excitatory and inhibitory postsynaptic potentials that are larger in magnitude) than those found in quiescent, resting states.

Our model, in agreement with other recent models, suggest that a single cortical network can shift between two dramatically different dynamical regimes that have traditionally been viewed as incompatible: criticality and asynchronous dynamics. By bridging the gap between these two points of view, we are optimistic that our results help resolve the debate over what kinds of dynamical regimes can manifest in the cortex.

2 Disrupted Cortical Dynamics and Motor Function in Freely Moving Rats due to E/I Imbalance and MeCP2 disruption

Abstract

Rett syndrome (RTT) is a devastating neurodevelopmental disorder, caused by disruptions to the MeCP2 gene, and resulting in severe cognitive and motor impairment. Previous work strongly suggests that healthy MeCP2 function is required to have a normal balance between excitatory and inhibitory neurons. However, the details of how neural circuit dynamics and motor function are disrupted remain unclear. How might imbalanced excitation/inhibition (E/I) cause problems for motor function in RTT? We addressed this question in the motor cortex of awake, freely behaving rats, comparing normal rats with a transgenic rat model of RTT. We recorded single-unit spiking activity while simultaneously recording body movement of the rats. We found that RTT rats tend to have excessive synchrony among neurons in the motor cortex and less complex body movements. Importantly, greater synchrony was correlated with greater stereotypy of relationships between neurons and body movements. To further test how our observations were related to an E/I imbalance, we pharmacologically altered inhibitory synaptic interactions. We were able to recapitulate many of the phenomena we found in MeCP2-deficient rats by enhancing inhibition in normal rats. Our results suggest that RTT-related E/I imbalance in the motor cortex gives rise to excessive synchrony and, consequently, a stereotyped motor code, which may underlie abnormal motor function in RTT.

2.1 Introduction

Rett syndrome (RTT), named after physician Andreas Rett, is a devastating postnatal neurodevelopmental disorder that affects various brain functions such as cognitive, sensory, emotional, motor and autonomic function [1]. RTT is mostly found in females with approximately 1 of every 10000 female births worldwide. Girls with RTT start to have developmental stagnation as early as six to eighteen months after birth, followed by rapid deterioration including loss of both communication skills and purposeful use of hands. Patients further develop autistic-like social behavior defects, cognitive impairment, motor abnormalities such as gait disturbances and stereotypical repetitive movements.

Due to the severity and frequency of RTT, decades of effort have been put into identifying the pathological mechanisms and clinical treatment of RTT. It has been identified that RTT is caused by mutations in the MeCP2 gene on the X chromosome, which encodes methyl-CpG binding protein 2 (MeCP2). MeCP2 is involved in the development of neuronal functions through neurogenesis, synaptic plasticity and establishment of neuronal circuits [2]. The loss of MeCP2 affects different cell types in multiple brain regions and developmental stages. On neural circuits level, the disruption of the MeCP2 gene in RTT alters the excitatory and inhibitory neurons differently, and thus complexly disturbs the excitation-inhibition (E/I) balance [57]. It has been found that MeCP2-mutant mice have excessive excitation over inhibition in visual cortex [58] and hippocampus [59], while a higher ratio of inhibition to excitation is found in primary somatosensory cortex and motor cortex of MeCP2-mutant mice [60, 61, 62]. Nevertheless, how the imbalance of excitation and inhibition affects the circuit mechanisms of motor cortex in RTT has largely remained unknown.

One important aspect of brain function is coordination among neurons. Orchestration of complex body movements requires some, but not too much, coordination among neurons in motor cortex; neither total synchrony nor total asynchrony will do. Indeed, theoretical studies have shown that excessive correlations can limit the information capacity of any neural code [63, 64, 65] - if all neurons are perfectly synchronized, then different neurons cannot encode different functions. Precisely how much and what kind of synchrony is best for motor coding and how motor function depends on changes in synchrony is poorly understood. It is well known, however, that the balance of excitation and inhibition plays a key role in modulating correlations among neurons. For instance, many computational models suggest that synchrony is strongly dependent on E/I interactions [21, 13, 66, 39]. Likewise, in experiments, pharmacological manipulation of E/I causes changes in synchrony [13, 17] and the excessive synchrony that occurs during epileptic seizures is often attributed to an E/I imbalance [67, 68]. Moreover, in our previous study, we found that the E/I imbalance alters the correlations among neurons in normal rat's primary motor cortex [69]. Thus, it is reasonable to hypothesize that the imbalance of excitation and inhibition in RTT leads to a dysfunctional coordination among neurons, and further causes abnormal motor function and behavior.

Here we test the hypothesis by recording neural activities and body movements simultaneously in primary motor cortex of rats under two conditions. First, we studied a transgenic rat model of Rett syndrome (RTT), which has disrupted expression of the MeCP2 gene. Second, we studied normal rats with acutely altered inhibitory neural interactions. Both these cases are associated with an imbalance of excitation and inhibition and, possibly, abnormal synchrony. Comparing MeCP2 disruption and excessive inhibition with the control

group (normal rats without altered inhibition), we show that both MeCP2 disruption and excessive inhibition lead to excessive synchrony in motor cortex. The degree of synchrony is correlated with the degree of abnormality of behavior and motor coding. Our findings suggest that RTT-related motor dysfunction may be due, in part, to excessive inhibition and synchrony in motor cortex.

2.2 Methods

2.2.1 Animals

We studied normal Sprague–Dawley male rats ($n = 3$, Harlan Labs, TX, USA) and transgenic MeCP2 knockout female rats ($n = 4$, HET KO, SD-Mecp2^{tm1sage}, Horizon Lab, MO, USA). The raw data from the normal rats was collected and first reported in our previous study [69], but reanalyzed here. The RTT rats have a 71 base pair deletion in Exon 4, and are maintained by breeding heterozygous females with wild type males, both with Sprague Dawley backgrounds. This animal model has been shown in other studies to recapitulate important dysfunctions and behaviors found in RTT humans including breathing abnormalities, unusual social interactions, exaggerated response to auditory stimuli, reduced gross locomotion, weak grip, and shortened lifespan [70, 71]. In addition, these rats have also been shown to manifest many of the same behavioral abnormalities found in some RTT mouse models including stunted body growth, maloccluded teeth, and reduced interest in social novelty [70]. All procedures followed the Guide for the Care and Use of Laboratory Animals of the National Institutes of Health and were approved by University of Arkansas Institutional Animal Care and Use Committee (protocol #14048).

2.2.2 Inhibitory modulation

To explore how the balance between inhibition and excitation influences the cortical states in Rett syndrome, we used two different drugs to systematically manipulate the level of inhibition. Both drugs target $GABA_A$ receptor, which respond to the major inhibitory neurotransmitter GABA. Muscimol is used as an agonist of $GABA_A$ receptor to increase the strength of inhibitory signaling, while Pentylenetetrazol (PTZ) is used as an antagonist of $GABA_A$ receptor to decrease the strength of inhibitory signaling.

The rats were given either 2 ml sterile saline or drug (muscimol or PTZ) diluted saline solution through intraperitoneal (IP) injection. For normal rats, the dose for muscimol was 2 mg/kg body weight; for RTT rats, we applied lower doses varying from 0.25 to 2 mg/kg body weight because these animals seemed to be more sensitive to excessive inhibition than normal rats. The dose for PTZ was 30 mg/kg body weight for both normal and RTT rats. After injection, we left 50 minutes before recording in order to let the drug sufficiently diffuses and affects the target region. The same waiting time was given to the control group for consistency, although pharmacologically unnecessary. On each recording day, we performed one no-drug recording first and then either one muscimol recording or one PTZ recording. The recordings were separated at least 1 hour for each rat.

2.2.3 Recording system setup

Since both neuronal activity and body movement are needed to examine the relationship between population coupling and body coupling, the recording system setup is designed to simultaneously record neuronal activity and body movement in freely moving rats. The recordings took place in a dark cubic space enclosed by black plastic boards, as shown in

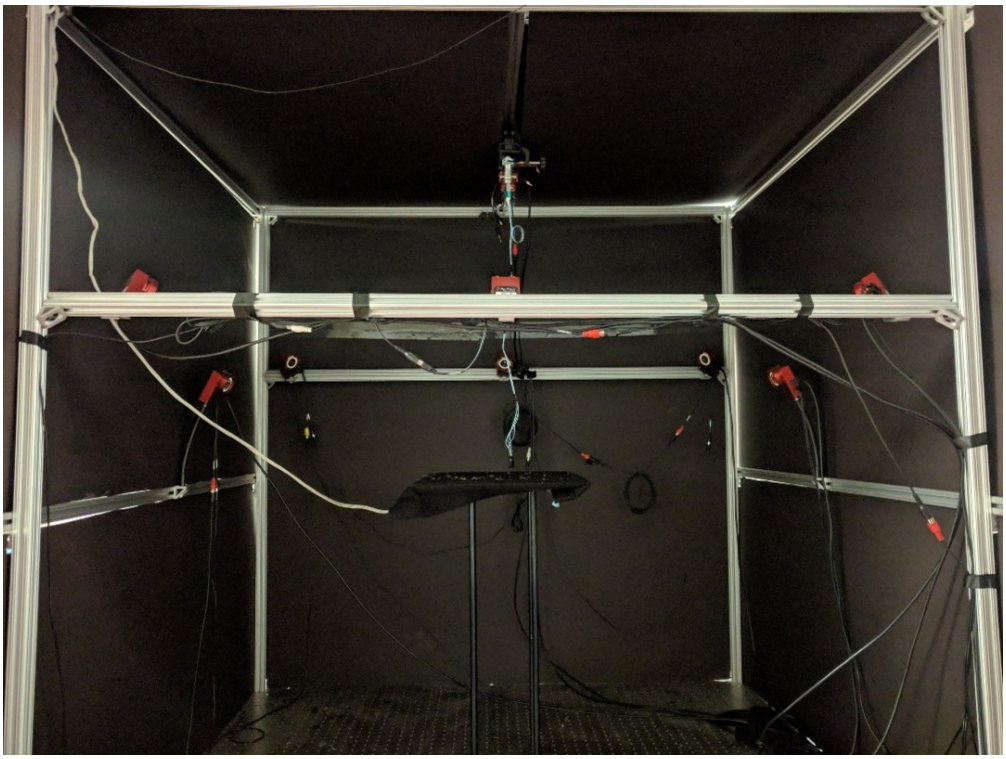

Figure 2.1: Recording system setup. The body tracking system consists of 8 infra-red cameras attached on the beams around the centered platform. The rats were able to to freely move on the platform placed at the center of the recording space. A lightweight cable with a proper length is used to connect the headstage of the electrode implanted on the rats to the neural recording system.

Fig. 2.1. During a 30-minute recording, the rats were allowed to freely move on a 30 cm $\times$ 30 cm platform placed at the center of the recording space. The platform is 2 feet height from the ground sustained by four pillars. 8 infra-red (IR) cameras are attached on the aluminum beams of the recording space. A commutator is attached on the ceiling of the recording space, with a lightweight cable to connect the headstage of the electrode on the rats. The length of the cable is carefully measured so that it does not impede the free movement of the rats. Each rat went through three acclimatization sessions before recording with the same setup to avoid stress and anxiety.

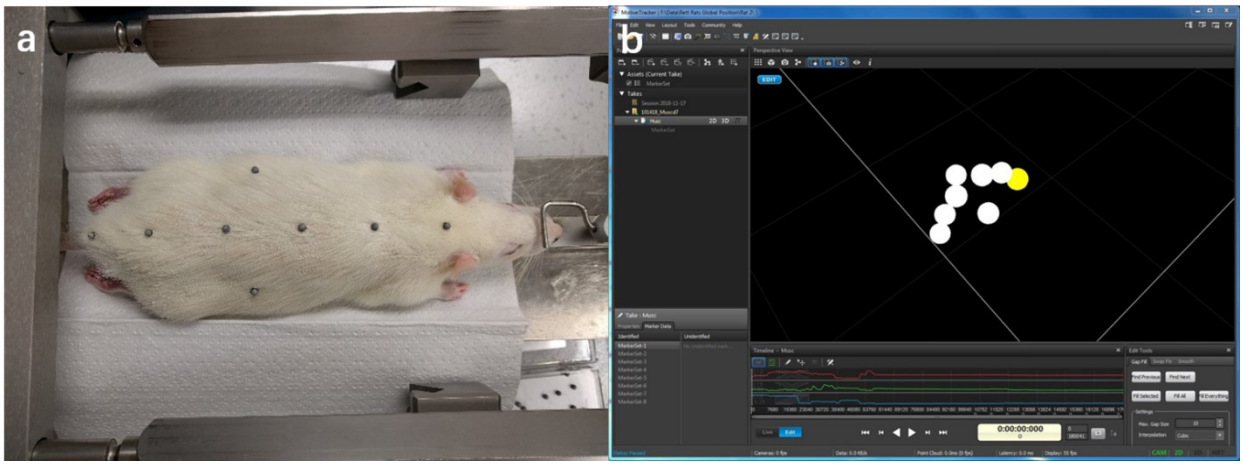

Figure 2.2: Body tracking setup. (a) Eight reflective beads were placed on the rats along the spine from neck to tail and on each lateral side of rear hips before recording. (b) Three-dimensional trajectories of the beads were tracked by the infra-red camera system, and were edited using Motive after recordings were completed.

2.2.4 Motion tracking

As in our previous work [69], body movement was recorded with a infra-red camera motion tracking system (OptiTrack Flex:V100R2). The motion tracking system captures the three-dimensional coordinate of eight reflective beads (MCP1125, Naturalpoint, 3 mm diameter) temporarily adhered on the rats along the spine from neck to tail and on each lateral side of rear hips, as shown in Fig. 2.2a. The tracking system has 10 ms time resolution and submillimeter spatial resolution. After recordings were completed, the tracking trajectories were manually corrected with the software, Motive (https://optitrack.com/software/motive), as shown in Fig. 2.2b. The tracking data was then smoothed by a 5 Hz low-pass filter in Matlab.

2.2.5 Electrophysiology

Microelectrode arrays were chronically implanted 1300 um deep in a 2 mm × 2 mm craniotomy with the center located 0.5 mm posterior to bregma and 2 mm lateral from midline, as shown in Fig. 2.3a-b. Thus, the recorded neurons were located in deep layers of the primary motor cortex and at positions associated with a wide range of body movements [72]. For the normal rat recordings, we used one type of microelectrode array (A8x4–2mm-200–200–413-CM32, Neuronexus); for RTT rats, we used a different type of microelectrode array (Buzsaki32-CM32, Neuronexus) for improved spike sorting [73]. For both groups, the plane of microelectrode arrays was oriented perpendicular to the dorsal surface and parallel to the midline. The craniotomy was closed with silicone adhesive (Kwik-Sil). To ensure the implantation is stable, 5 holes were drilled peripheral to the craniotomy and screws were half-way deep placed in the holes, as shown in Fig. 2.3c. Dental cement was applied to adhere and cover the exposed area, where an anchor was included beside the probe to keep the connector tightly connected to the probe during recordings, as shown in Fig. 2.3d.

After implantation surgery, the rats recovered for at least 2 weeks before recordings began. During each 30-minute recording, extracellular voltage fluctuations were recorded with 30 kHz sample rate (Cerebus, Blackrock Microsystems), as shown in Fig. 2.4. Signals were digitized by a headstage connected to the electrode, and transmitted by a commutator connected to the recording system. Spike sorting was done with the Kilosort (https://github.com/cortex-lab/KiloSort), a fast and accurate spike sorting algorithm for high-channel count probes [74]. Then, we manually curated the spike sorting results with the graphical user interface Phy (https://github.com/cortex-lab/phy), as shown in Fig. 2.5.

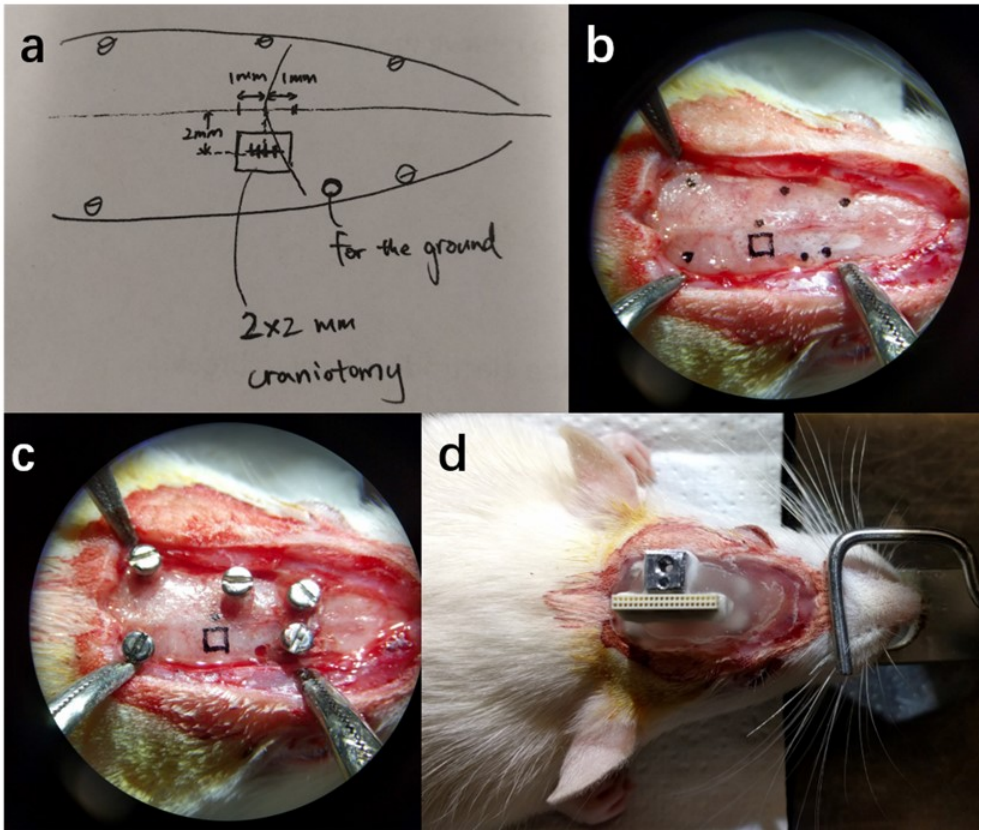

Figure 2.3: Chronic implantation surgery. (a) Location of craniotomy and screws. (b) Marked location of craniotomy and screws on skull. (c) Half-way drilled screws peripheral to the craniotomy. (d) Implanted probe and anchor covered by dental cement.

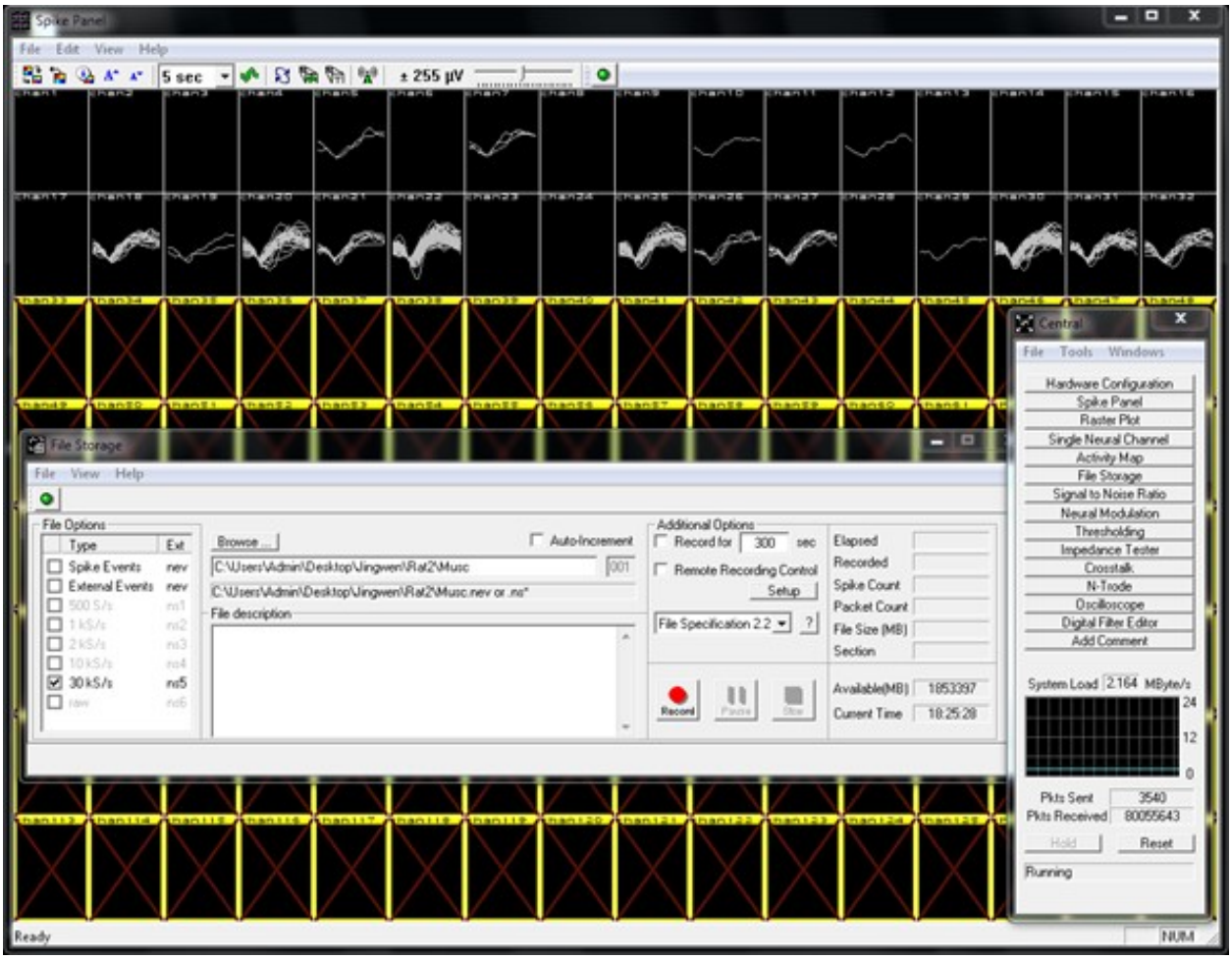

Figure 2.4: Signals shown on the Blackrock Microsystems interface during recording.

Criteria for a good unit included clear and distinct waveform shapes, refractory periods in auto-correlograms, stability in amplitudes, and distinct principal components in feature space (Fig. 2.6).

2.2.6 Body tracking data analysis

We considered two aspects of body movement: general motility and complexity of movements. We used the distance traveled by the rat during the recording to represent the

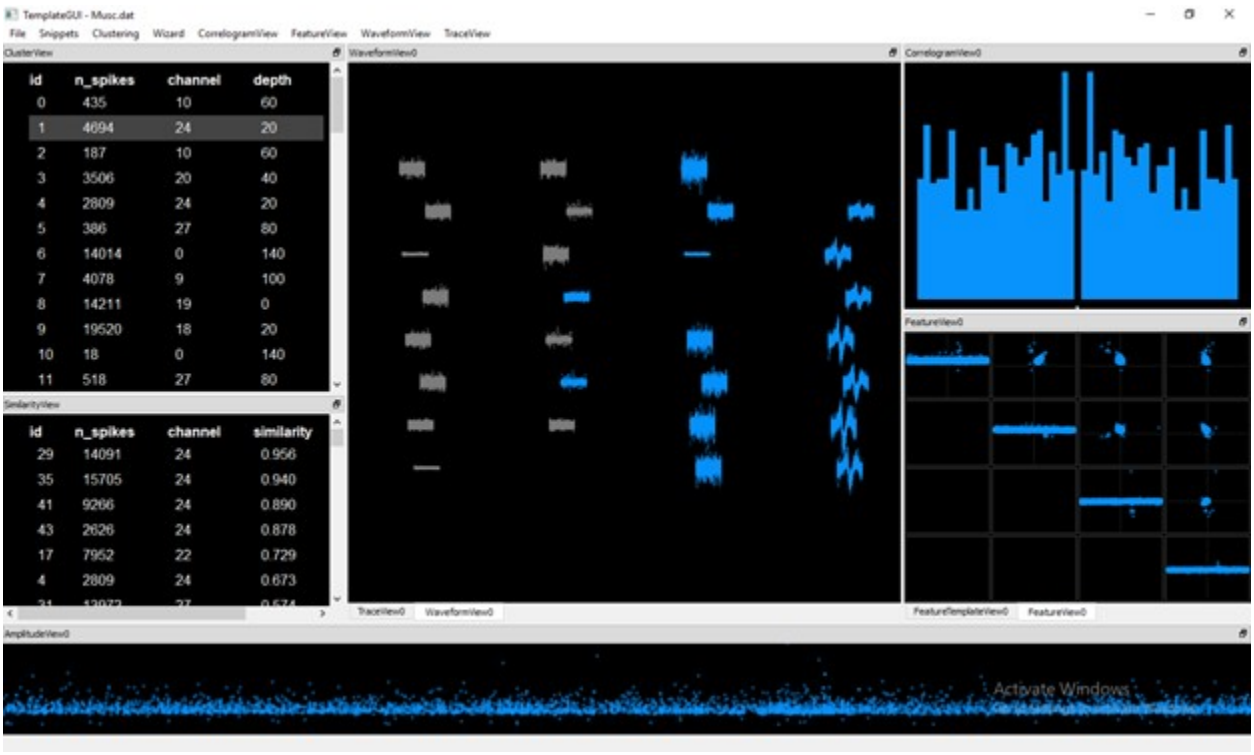

Figure 2.5: Graphical user interface Phy for manually curated the spike sorting results.

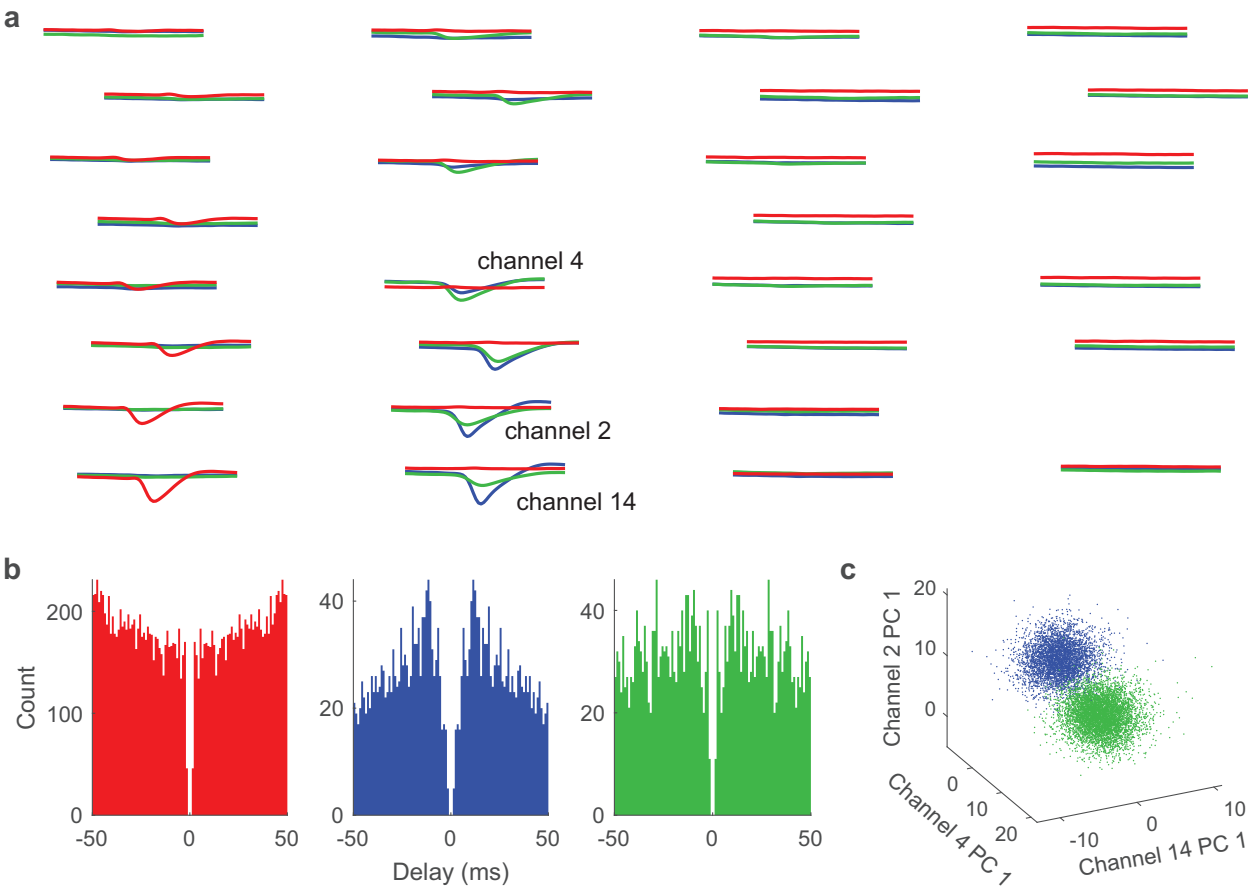

Figure 2.6: **Example of good units in spike sorting.** a, Spike waveforms for three units (red, blue, and green) on the electrodes. The three units are distinguished by the spike sorting algorithm based on the different spike waveforms across channels. b, Autocorrelograms for the spike times of the three units. The gap near zero delay indicates the refractory period expected for a single unit. c, Principle component analysis of spike waveform helps the spike sorting algorithm to distinguish different units. Each point represents a spike. The two units (blue and green) are well separated in the principle component space of certain channels.

general motility. The distance traveled was calculated for each recording as the cumulative distance traveled by the center of mass of the tracking beads. Complexity of movements was assessed by principle component analysis on the speed of 8 beads. The speed of center of mass and beads were then obtained by calculating differentiated positions. Time periods when the rats were at rest for more than 1.5 s were excluded. We defined the animal to be 'at rest' if it met two conditions: 1) speed of center of mass less than 0.8 cm/s; 2) speed of each bead less than 1 cm/s. Brief periods of motion, shorter than 0.5 s, preceded and followed by rest were considered rest. After excluding rest periods and applying principle component analysis, we counted the number of principal components that explains 95 percent of variance, defined as N95. If only a few principal components are needed to explain most of the variance, the data is largely correlated and low-dimensional; if more principal components are needed to explain the variance, the data is more complex and high-dimensional. Thus, the N95 we defined represents the complexity of movements.

2.2.7 Spiking data analysis

We examined a few aspects of the spiking data: spike rate, synchrony, cortical stereotypy, and motor stereotypy. While synchrony directly measures correlations in the spiking activity among neurons, cortical stereotypy reveals more detailed temporal structures in spike timing among neurons. Motor stereotypy captures the interaction between neural activities and body movements.

Specifically, spike rate of a recording was obtained by the average spike rate across all units during the recording. Synchrony is defined as the average of pairwise correlations of spike count time series across all pairs of neurons. The spike count time series were calculated

for each neuron using 1 second time bin.

Cortical stereotypy is defined to capture stereotypy in intracortical interactions (ICI). For each neuron (trigger neuron), we counted the number of spikes from the population (with 10 ms time bin) in a ± 1 second time window centered on the spike times of the trigger neuron. We then averaged these spike-triggered spike count waveforms across all spikes from the trigger neuron to obtain the ICI waveforms. Cortical stereotypy was calculated by averaging pairwise correlations of ICI waveforms across all pairs of units as a single number for each recording.

Motor stereotypy is defined to capture stereotypy in body-cortex interactions (BCI). Similar to ICI waveform, we obtained a BCI waveform for each neuron (the trigger neuron) by averaging the speed of center of mass in a ± 1 second time window centered on the spike times of the trigger neuron. The waveform was then smoothed by a 1.5 Hz low pass filter and normalized by its mean. Motor stereotypy is defined as the average of pairwise correlations of BCI waveforms across all pairs of units to obtain a single number for each recording.

2.2.8 Statistics

We examined the statistical significance of the difference between different groups using p-value of t-tests. The p-value represents the probability of accepting the null hypothesis that the means of two groups are not different. For correlations, we used the correlation coefficient and its corresponding p-value to test the statistical significance of correlations between two quantities. The p-value represents the null hypothesis that the two quantities are uncorrelated.

2.3 Results

We performed experiments with rats freely behaving, e.g. walking, grooming, and changing posture, on a 30 cm $\times$ 30 cm platform inside a dark enclosure as shown in Fig. 2.7a. We simultaneously recorded body movements and spiking activity of many single neurons in motor cortex during each 30 minute recording (Fig. 2.7b). Our goal is to quantitatively assess differences in body movements, neural activity, and the neuron-to-body relationship of different experimental groups: wild-type rats and RTT rats with different pharmacological manipulation.

In this section, we first compared wild-type rats, wild-type rats with enhanced inhibition (Muscimol), and RTT rats. We expected to see that enhanced inhibition in normal rats and RTT rats causes deviation in the same direction compared to normal rats. We also included RTT rats with enhanced inhibition in comparison to validate if it pushes the deviation further from normal rats. We then compared wild-type rats and RTT rats with reduced inhibition (PTZ) to see if reduced inhibition in RTT rats could tune the neural activity, neuron-to-body relationship, and behavior back towards normal.

We obtained $n = 255$ recordings with at least 8 good units in total. Among them, there are $n = 39$ recordings for wild-type rats with no drug, $n = 17$ recordings for wild-type rats with muscimol, $n = 20$ recordings for wild-type rats with PTZ, $n = 86$ recordings for RTT rats with no drug, $n = 37$ recordings for RTT rats with muscimol 0.25 mg/kgbw, $n = 14$ recordings for RTT rats with muscimol 0.5-2 mg/kgbw, and $n = 42$ recordings for RTT rats with PTZ. After spike sorting (Kilosort [74]), we obtained 6685 single units in total ($n = 27$ units per recording on average).

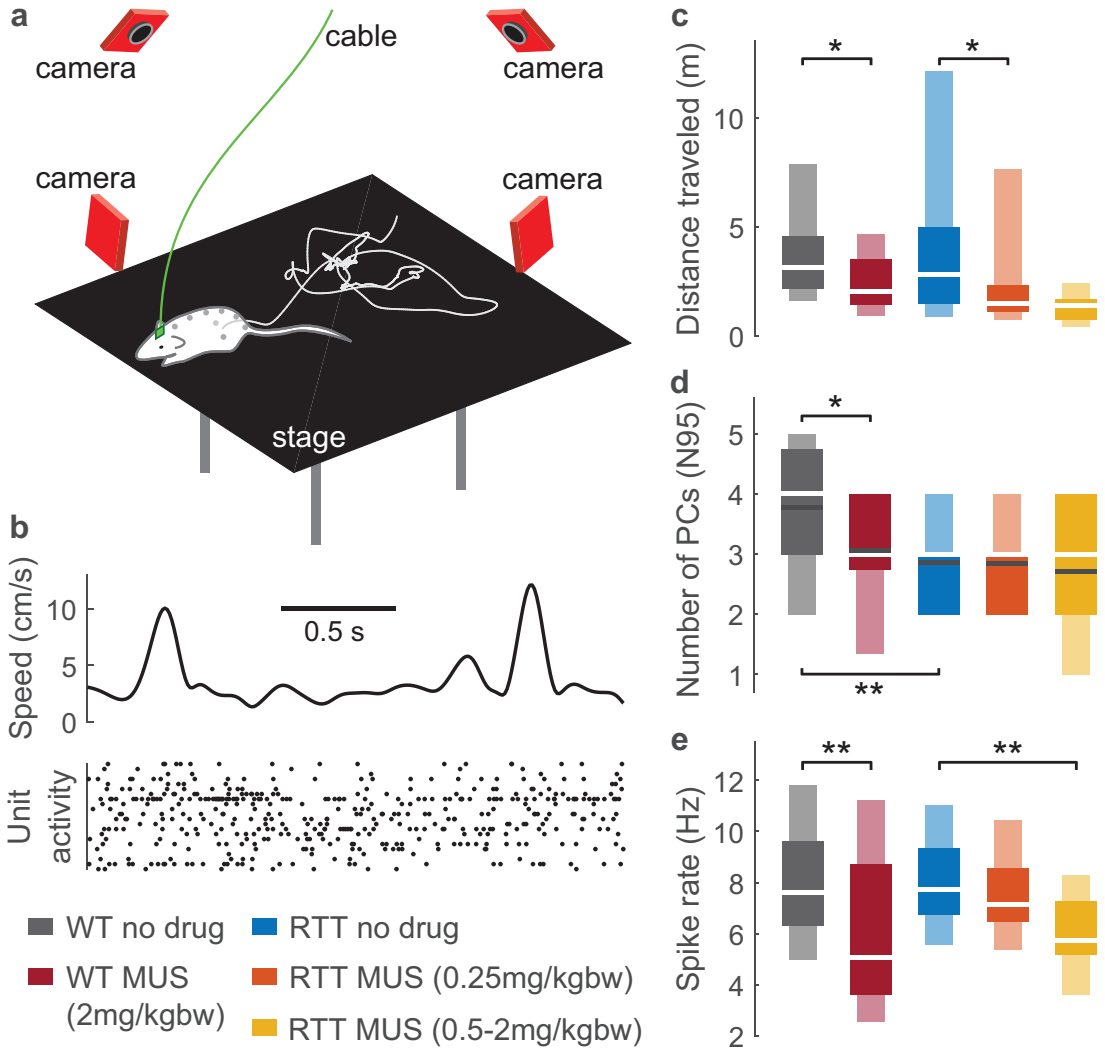

Figure 2.7: **Reduced behavioral complexity due to MeCP2 disruption and excessive inhibition in motor cortex.** a, An example movement path (white line) of a rat, obtained by tracking the positions of eight beads attached to the rat. b, Body speed and single unit neural activity were recorded simultaneously. c, Both wild-type (WT) rats and RTT rats moved less due to enhanced inhibition (WT no drug vs. MUS: $p = 0.022$; RTT no drug vs. MUS low dose: $p = 0.017$). d, Complexity of movements is reduced for RTT rats compared to WT rats ($p < 0.001$). The reduced complexity is also found in WT rats with enhanced inhibition ($p = 0.018$). e, Spike rate is reduced for enhanced inhibition (WT no drug vs. MUS: $p = 0.010$; RTT no drug vs. MUS high dose: $p < 0.001$), but is not different between WT and RTT rats ($p = 0.978$). In c-e, asterisks indicate t-test significance: $^*p < 0.05$, $^{**}p < 0.01$. Dark and light boxes delineate 0.25-0.75 and 0.05-0.95 quantiles, respectively. White lines mark median. Black lines mark mean in d.

2.3.1 Behavior

We first examined general motility of the rats. We used the speed of representative beads to calculate the total distance traveled by the center of mass during the 30 min recording, and found that administering muscimol resulted in reduced animal motility (Fig. 2.7c). Although RTT rats were more variable, they did not exhibit significantly different amount of movement on average compared with normal rats (Fig. 2.7c).

However, a more subtle analysis revealed that RTT rats exhibited less complex (i.e. lower dimensional) body movement compared to normal rats (Fig. 2.7d). We assessed complexity of movements based on principle component analysis of the 8-dimensional bead speed data, considering only times when the animal was active to avoid confounding movement complexity with general motivation to move (see Methods). We counted how many principal components were needed to account for 95 percent of the variance of bead speed fluctuations; we called this count N95. We found that normal rats moved with more complex, higher dimensional body motion, requiring significantly more principal components (greater N95) than RTT rats. In addition, we found that, when muscimol was applied, the average N95 of normal rats dropped to a similar level as RTT rats. Thus, we found a less complexity of movement in RTT rats and normal rats with enhanced inhibition compared to normal rats.

2.3.2 Spike rate

Next, we analyzed our neural recordings seeking correlates of the reduced complexity in behavior induced by MeCP2 disruption and excessive inhibition. We first looked at the basic statistics of neural activities, i.e. spike rate. We compared spike rates across the

different experimental groups. We found that muscimol resulted in decreased spike rates for both normal and RTT rats (Fig. 2.7e). However, the difference in spike rates between normal and RTT rats was not significant (Fig. 2.7e). Thus, other measurements are needed to capture the difference in neural activities between normal and RTT rats.

2.3.3 Synchrony

We examined correlations in the spiking activity. For each recording, we computed the correlation of every pair of simultaneously recorded neurons (Fig. 2.8a) and then averaged these pairwise correlations across all pairs (Fig. 2.8b) to obtain a single number, called 'synchrony' in Fig. 2.8c (more detail in Methods). Although synchrony varied greatly across recordings, we found a significant increase in synchrony for the RTT rats compared to the normal rats. Similarly, application of muscimol resulted in a large increase in synchrony for both normal and RTT rats. This result is somewhat surprising considering that stronger inhibition is often associated with reduced synchrony in theory [21, 75] and GABA agonists can result in reduced synchrony [13], but our finding is consistent with a recent study that applied muscimol in motor cortex of awake rats [69]. In conclusion, we found a higher synchrony in motor cortex for RTT and enhanced inhibition.

These results suggest that the increased synchrony we observed in RTT rats and for enhanced inhibition could be responsible for reduced behavioral complexity. Consistent with this possibility, we found that synchrony was negatively correlated with distance traveled (Fig. 2.8d) and behavioral dimensionality N95 (Fig. 2.8e). Thus, we concluded that higher synchrony in M1 is related to reduced mobility and reduced movement complexity.

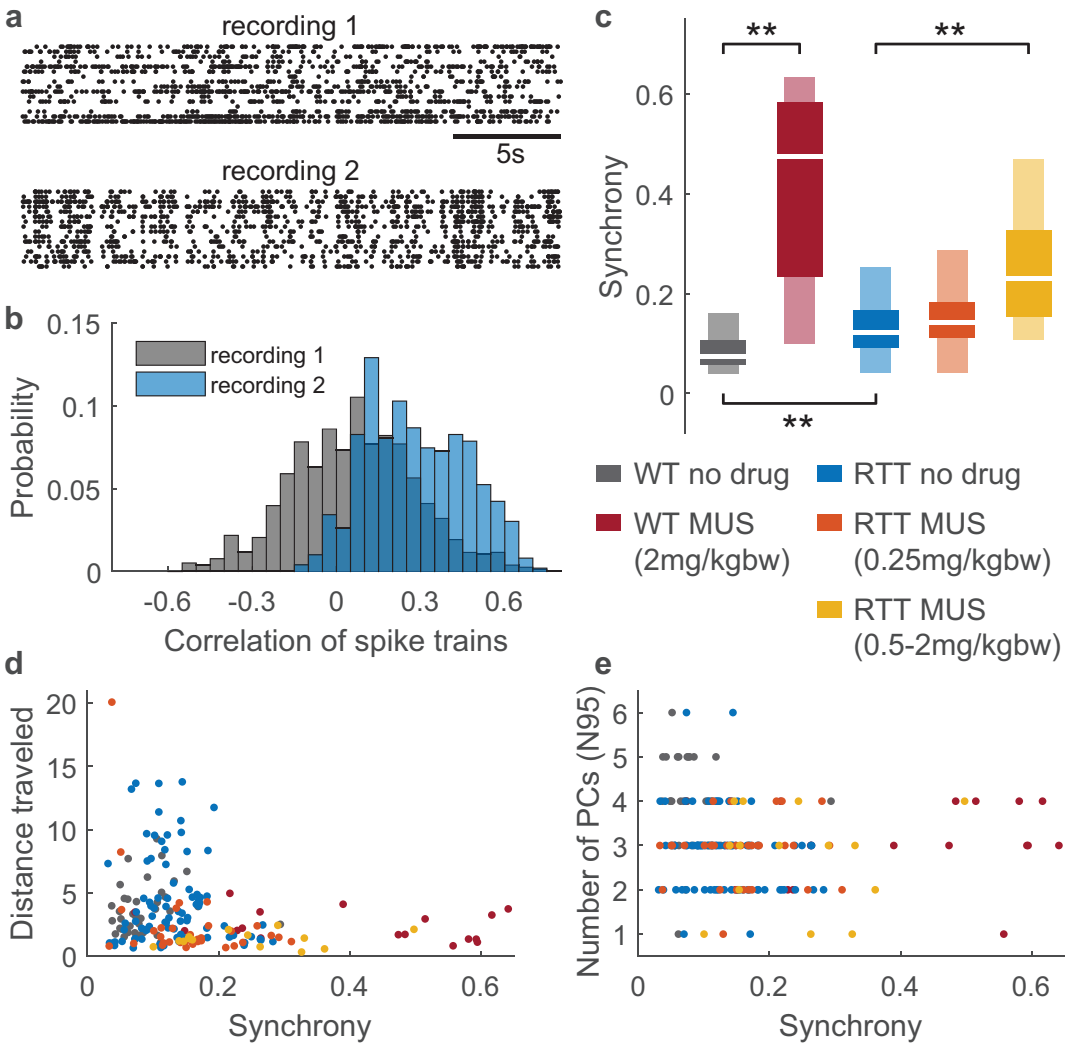

Figure 2.8: **Increased synchrony due to MeCP2 and excessive inhibition correlates to reduced behavioral complexity.** a, Example spike rasters from a WT no drug recording (recording 1) and a RTT no drug recording (recording 2) show different level of correlations. b, Distributions of pairwise correlations of spike trains reveal larger correlations on average in recording 2 compared to recording 1. We defined the average across all pairs as 'synchrony'. c, Summary of all recordings shows increased synchrony in RTT rats compared to WT rats ($p < 0.001$). Similarly, increasing inhibition results in increased synchrony (WT no drug vs. MUS: $p < 0.001$; RTT no drug vs. MUS high dose: $p < 0.001$). Asterisks indicate t-test significance: $^{**}p < 0.01$. Dark and light boxes delineate 0.25-0.75 and 0.05-0.95 quantiles, respectively. White lines mark median. d, Mobility is negatively correlated with synchrony (Pearson $\rho = -0.21$, $p = 0.003$). e, Complexity of movements is negatively correlated with synchrony (Spearman $\rho = -0.22$, $p = 0.002$). Color represents different groups in d and e.

2.3.4 Cortical stereotypy

The synchrony results presented in Fig. 2.8 provide a limited view of the relationships among neurons. In particular, such average pairwise correlations assess instantaneous relationships and miss any temporally structured interactions among neurons, which may be important if spike timing matters for motor coding. To better account for such temporal relationships, we next examined spike-triggered average histogram waveforms of population activity for each neuron (Fig. 2.9a); hereafter we refer to these as intracortical interaction (ICI) waveforms. Similar to previous studies of population coupling [76, 69, 77], we define the population activity as the spike count time series of all recorded neurons, excluding the trigger neuron (the one whose spike times are used to do the spike-triggered average). The shape of an ICI waveform reveals whether and how the trigger neuron leads or lags the activity of the network in which it is embedded. A flat line in the ICI waveform would indicate a neuron that fires independently of the population. After obtaining an ICI waveform for each single neuron, we then compared ICI waveforms across neurons. We found that for normal rats, ICI waveforms were diverse; some neurons lead, others lag the population; some neurons had sharply peaked ICI waveforms, others had broader peaks (Fig. 2.9a, gray). In contrast, in the RTT rats, neurons tended to have stereotyped ICI waveforms (Fig. 2.9a). This means that each neuron tends to participate with the population in the same way in RTT M1. We quantified this cortical stereotypy by calculating correlations between all pairs of ICI waveforms (Fig. 2.9b) for each recording and then averaging across all pairs, to obtain a single ICI stereotypy number for each recording. Comparing across our experimental groups, we found that ICI stereotypy was much greater in RTT rats than in normal rats

(Fig. 2.9c). Similarly, we found that application of muscimol resulted in greatly increased ICI stereotypy for both normal and RTT rats (Fig. 2.9c). We conclude that diversity of temporal relationships among neurons in M1 is compromised in MeCP2 deficient rats in a way that is consistent with an increase in inhibition in M1.

Given the conceptual similarity between synchrony and ICI stereotypy, one might expect that these two quantities are directly linked. However, we found that synchrony and ICI stereotypy were nearly uncorrelated for normal rats (Fig. 2.9d). In contrast, for RTT rats and for normal rats with increased inhibition, synchrony is strongly correlated with ICI stereotypy (Fig. 2.9d). We conclude that, even though synchrony can be high in normal rats, this 'normal synchrony' does not come with stereotyped intracortical interactions.

2.3.5 Motor stereotypy

So far, we have shown reduced complexity of neural activity (i.e. higher synchrony and greater ICI stereotypy) and reduced complexity of behavior (lower N95) in RTT rats compared to normal rats. Since neurons in M1 influence the body movements of these animals, it stands to reason that the relationships between neurons and body movements, i.e. the motor code, might also be compromised and less complex in RTT rats. Alternatively, it could be that higher-level decision making or movement planning circuits are altered in RTT rats, and that motor coding remains intact. To begin to distinguish these possibilities, we next measured stereotypy of body-cortex interactions (BCI). Similar to our approach with ICI stereotypy, we calculated spike-triggered average waveforms of body speed - termed BCI waveforms (Fig. 2.10a, more details in methods). We obtained one BCI waveform for each neuron. A complex motor code would manifest with different neurons firing in relation

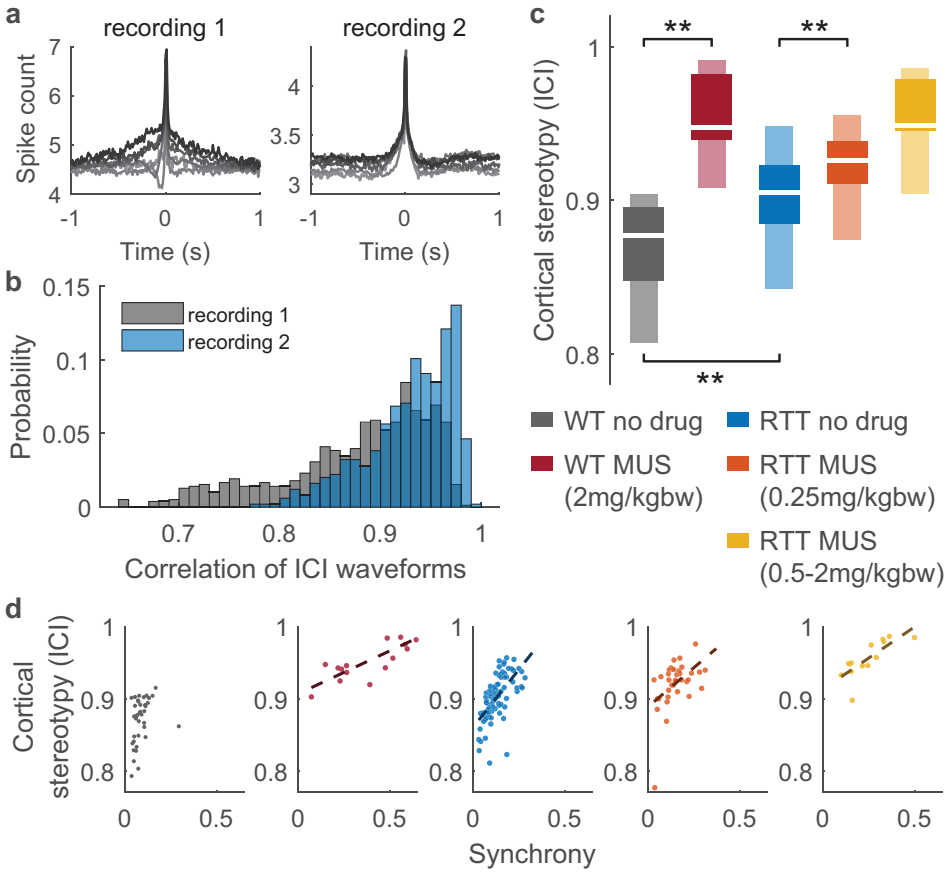

Figure 2.9: **Stereotyped interactions among M1 neurons due to MeCP2 disruption and excessive inhibition.** a, Spike-triggered average population acitivity (i.e. ICI waveform) for six example neurons from a WT rat (recording 1) and from a RTT rat (recording 2). Stereotyped ICI waveforms in recording 2 indicate that intracortical interactions are less diverse than in recording 1. b, ICI waveforms were compared for each pair of neurons. Distributions of pairwise correlations of ICI waveforms reveal greater diversity of waveforms in recording 1 compared to recording 2. We defined the average across all pairs as 'cortical stereotypy'. c, Summary of all recordings shows that RTT rats have greater cortical stereotypy than WT rats ($p < 0.001$). Increased cortical stereotypy is also caused by enhanced inhibition (WT no drug vs. MUS: $p < 0.001$; RTT no drug vs. MUS low dose: $p = 0.002$). Asterisks indicate t-test significance: $^{**}p < 0.01$. Dark and light boxes delineate 0.25-0.75 and 0.05-0.95 quantiles, respectively. White lines mark median. d, Excessive synchrony links to increased cortical stereotypy for RTT rats and enhanced inhibition. Cortical stereotypy and synchrony are nearly uncorrelated for WT rats ($\rho = 0.32$, $p = 0.046$), but strongly correlated in RTT rats ($\rho = 0.61$, $p < 0.001$) and enhanced inhibition (WT MUS: $\rho = 0.83$, $p < 0.001$; RTT MUS low dose: $\rho = 0.47$, $p = 0.003$; RTT MUS high dose: $\rho = 0.78$, $p = 0.001$). Color represents different groups. Dashed lines show the best linear fit when $p < 0.01$.

to different aspects of body movement, i.e. diverse BCI waveforms across neurons. For each recording session, we quantified stereotypy of BCI waveforms by calculating the average pairwise correlation of all BCI waveforms (Fig. 2.10b). Similar to our ICI stereotypy results, we found that BCI waveforms were very diverse in normal rats - BCI stereotypy was low (Fig. 2.10c). In RTT rats, BCI stereotypy was highly variable and slightly increased on average compared to normal rats, but not significantly. However, the extreme values of BCI stereotypy (say, above 0.7) that we saw in some RTT rats never occurred for normal rats. Increased inhibition resulted in dramatic increases in BCI stereotypy for both normal and RTT rats. How does BCI stereotypy relate to synchrony? Similar to ICI stereotypy, we found that BCI stereotypy was strongly correlated with synchrony for RTT rats and for conditions with excessive inhibition (Fig. 2.10d). Moreover, for normal rats, BCI stereotypy was not significantly correlated with synchrony. We conclude that the synchrony that occurs naturally among healthy M1 neurons does not entail a low-dimensional motor code like it does in RTT rats and for excess inhibition.

2.3.6 Reduced inhibition

Next, we applied all the analysis above on normal rats and RTT rats with reduced inhibition (PTZ) to further explore the role of inhibition in our RTT rat model. Our original motivation for this was the possibility of rescuing normal motor function in RTT rats. However, we found that partially blocking inhibition did not recover normal motor function as shown below.

The total distance traveled by the rats with reduced inhibition is significantly increased, for both normal rats and RTT rats (Fig. 2.11a). The complexity of movements,

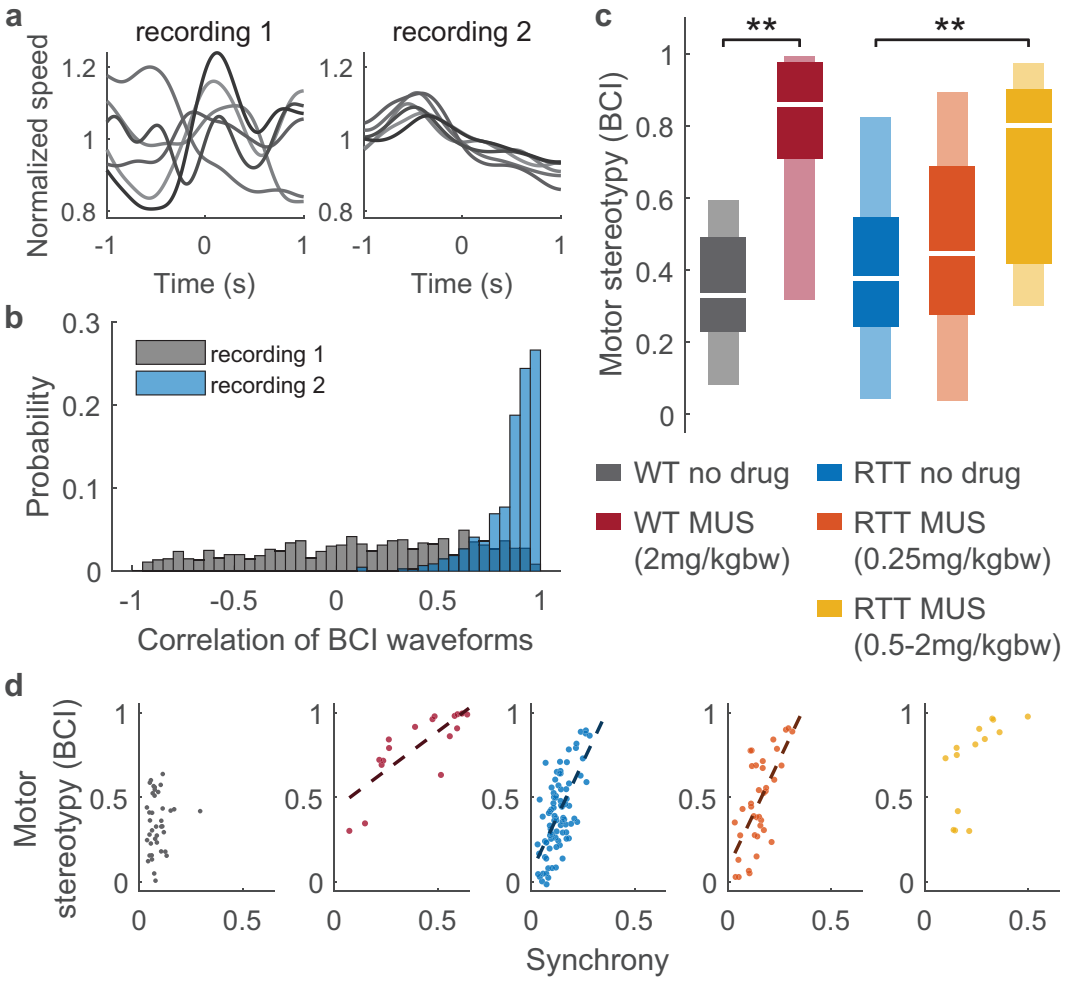

Figure 2.10: **Stereotyped body-cortex interaction due to MeCP2 disruption and excessive inhibition.** a, Each line (BCI waveform) is a spike-triggered average of body speed from one neuron. These example BCI waveforms are more diverse for the WT rat (recording 1) than for the RTT rat (recording 2). b, Summary of BCI waveform similarity (correlation) for all pairs of neuron in recording 1 compared to recording 2. We defined the average across all pairs as motor stereotypy. c, Enhanced inhibition caused increased motor stereotypy (WT no drug vs. MUS: $p < 0.001$; RTT no drug vs. MUS high dose $p < 0.001$). Asterisks indicate t-test significance: $^{**}p < 0.01$. Dark and light boxes delineate 0.25-0.75 and 0.05-0.95 quantiles, respectively. White lines mark median. d, Synchrony correlates with motor stereotypy for RTT rats ($\rho = 0.66$, $p < 0.001$) and enhanced inhibition (WT MUS: $\rho = 0.80$, $p < 0.001$; RTT MUS low dose: $\rho = 0.72$, $p < 0.001$; RTT MUS high dose: $\rho = 0.65$, $p = 0.012$), but not for WT rats ($p = 0.558$). Note that extreme values of motor stereotypy (¿0.7) were not observed in normal rats. Color represents different groups. Dash lines show the best linear fit when $p < 0.01$.

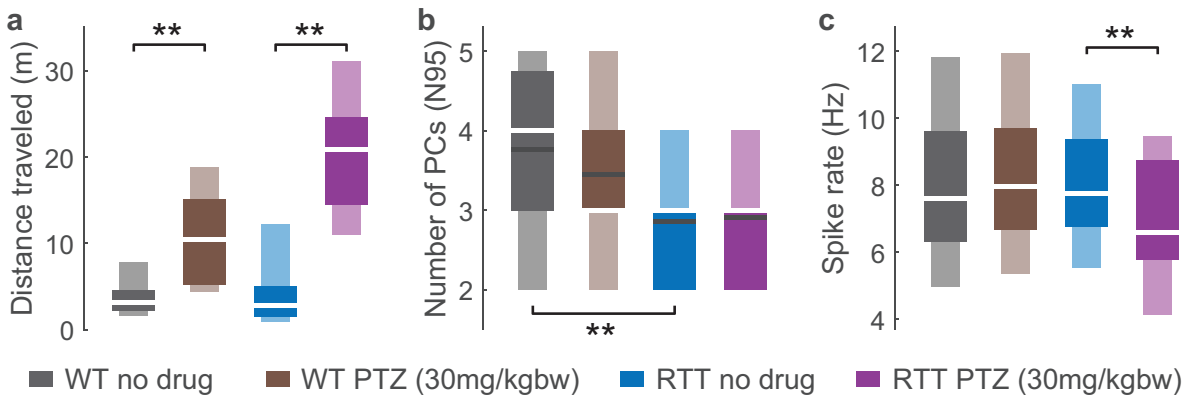

Figure 2.11: **Mobility, complexity of movements, and spike rate for normal rats and RTT rats with reduced inhibition.** a, Wild-type (WT) rats and RTT rats moved much more due to PTZ application (WT no drug vs. PTZ: $p < 0.001$; RTT no drug vs. PTZ: $p < 0.001$). The increase for RTT rats was larger than for WT rats. b, No significant difference in complexity of movements was found for reduced inhibition (WT no drug vs. PTZ: $p = 0.246$; RTT no drug vs. PTZ: $p = 0.774$). c, Spike rate is not different in WT rats with reduced inhibition ($p = 0.827$), but is reduced in RTT rats with reduced inhibition ($p = 0.001$). Asterisks indicate t-test significance: $^{**}p < 0.01$. Dark and light boxes delineate 0.25-0.75 and 0.05-0.95 quantiles, respectively. White lines mark median. Black lines mark mean in b.

however, is not affected by reduced inhibition (Fig. 2.11b). Furthermore, reduced inhibition does not cause difference in spike rate for normal rats, but decreases spike rate for RTT rats (Fig. 2.11c).

We examined synchrony, cortical stereotypy (ICI), motor stereotypy (BCI) for normal rats and RTT rats with reduced inhibition. While reduced inhibition decreases synchrony in RTT rats and pushes it back towards synchrony in normal rats (Fig. 2.12a), it does not cause significant difference in ICI stereotypy and BCI stereotypy for RTT rats (Fig. 2.12b-c). Moreover, while reduced inhibition turns the relationship of ICI stereotypy and synchrony uncorrelated in RTT (Fig. 2.12d), BCI stereotypy and synchrony stays significantly correlated for RTT rats with reduced inhibition (Fig. 2.12e). Thus, we concluded that reducing inhibition with PTZ does not recover normal motor function.

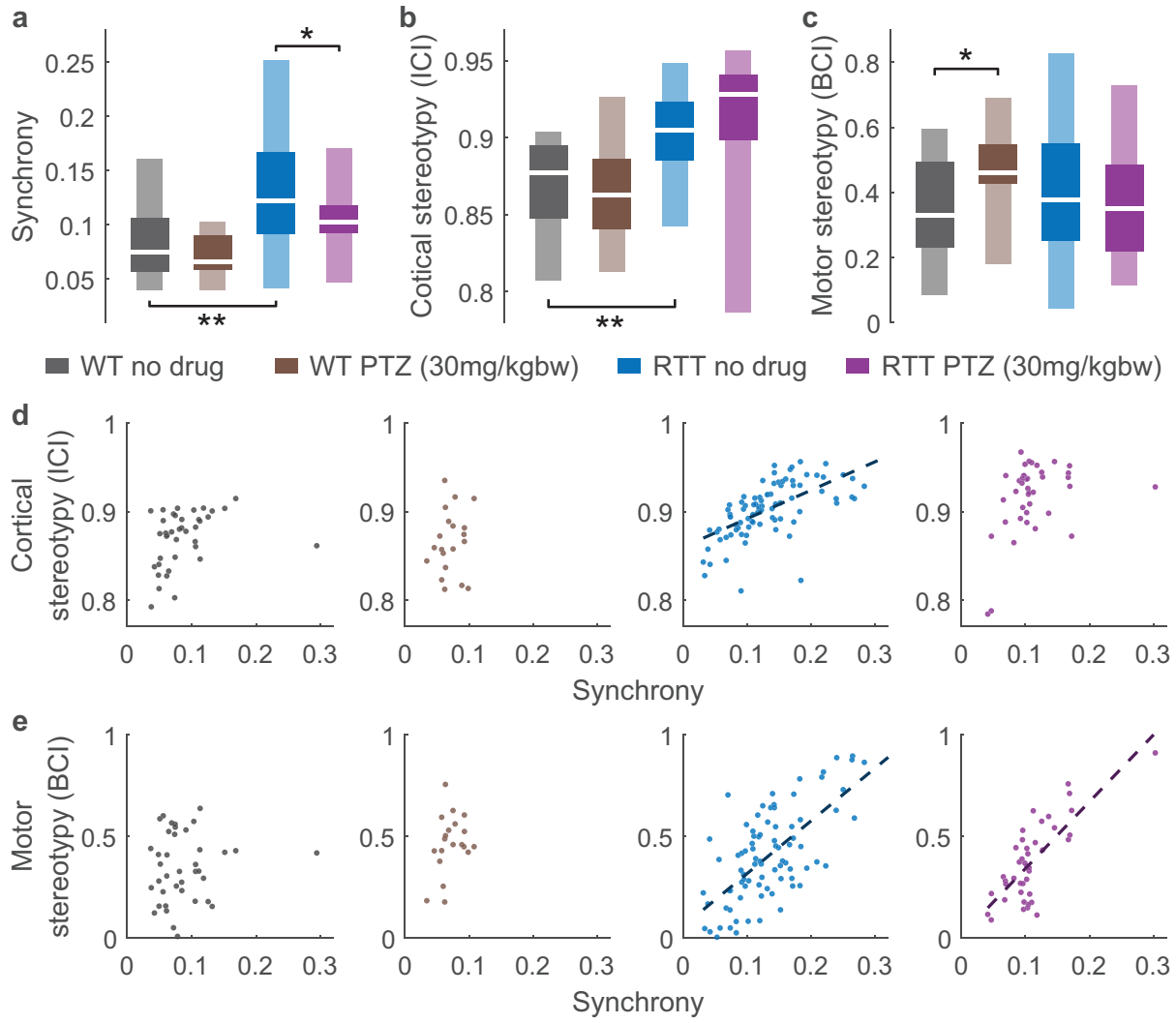

Figure 2.12: **Synchrony, cortical stereotypy, motor stereotypy, and their correlations for normal rats and RTT rats with reduced inhibition.** a, Synchrony is not significantly changed by PTZ for WT rats ($p = 0.146$), but decreases in RTT rats with reduced inhibition ($p = 0.031$). b, No significant difference is found in cortical stereotypy for reduced inhibition (WT no drug vs. PTZ: $p = 0.587$; RTT no drug vs. PTZ: $p = 0.111$). c, Reduced inhibition caused increased in motor stereotypy for WT rats ($p = 0.010$), but not for RTT rats ($p = 0.475$). In a-c, asterisks indicate t-test significance: $^*p < 0.05$, $^{**}p < 0.01$. Dark and light boxes delineate 0.25-0.75 and 0.05-0.95 quantiles, respectively. White lines mark median. d, Cortical stereotypy and synchrony stayed uncorrelated for WT rats with reduced inhibition ($p = 0.552$). For RTT rats, the correlation of cortical stereotypy and synchrony was weakened with reduced inhibition ($\rho = 0.38$, $p = 0.012$). e, Motor stereotypy and synchrony stayed uncorrelated for WT rats with reduced inhibition ($p = 0.160$), and stayed correlated for RTT rats with reduced inhibition ($\rho = 0.76$, $p < 0.001$). In d-e, color represents different groups. Dash lines show the best linear fit when $p < 0.01$.

2.4 Discussion

Here we have shown that MeCP2 disruption and increased inhibition cause a similar reduction in complexity of the motor system. Compared to normal rats with intact inhibition, this reduced complexity manifested in four ways: body movements were simpler (lower dimensional), neural activity became less diverse (i.e. more synchronous) across the neural population in M1, interactions among neurons in M1 became more stereotyped, and relationships between M1 neurons and body movements became more stereotyped. Returning to the questions we posed at the start, one interpretation of our observations is that MeCP2 disruptions cause an imbalance favoring inhibition in M1, which results in excessive neural synchrony, thereby limiting the information capacity of the motor code; the commands sent to the spinal cord from M1 are less diverse. In this view, the reductions in complexity of behavior and neuron-to-body relationships are a natural consequence of the less complex commands issued from neurons in M1.

However, our more careful look at our results adds nuance to this interpretation. Elevated synchrony in M1 does not always coincide with a general reduction in complexity of the motor system. Indeed, our measurements demonstrate that normal healthy rats exhibit a wide range of synchrony, varying greatly from one recording to another. As shown in Fig. 2.8c, the 5%-95% range of measured synchrony values in normal rats was 0.04-0.16, which overlaps substantially with the 5%-95% range measured in RTT rats - 0.04-0.25. But, even the highest levels of synchrony we observed in normal healthy rats did not come with dramatic reductions in motor complexity. Considering this fact, a more accurate conclusion from our results would be that enhanced inhibition and MeCP2 disruption result in a dysfunctional

type of synchrony, that reduces motor complexity and is different from the synchrony found in healthy M1 circuits. In agreement with this idea, previous work has highlighted the beneficial role of synchrony in M1, "binding" functional groups of neurons which are associated with distinct muscle groups [78, 79] or motor planning [80]. Our measurements of ICI stereotypy suggest that one way in which this unhealthy synchrony differs from normal synchrony lies in the temporal aspects of relationships among neurons. Very high ICI stereotypy (above 0.9), which was not observed in our recordings of normal rats, implies that all neurons have very similar temporal relationships - firing with the same lag or lead relative to the population. In the normal rats, high synchrony could coexist with diverse temporal relationships among neurons.

Application of muscimol in normal rats recapitulated many of our observed differences between RTT rats and normal rats. This observation is consistent with previous studies that point to an imbalance favoring too much inhibition in forebrain areas as a circuit-level problem associated with RTT [60, 61, 62]. However, this observation also deserves more careful attention. Not all aspects of our measurements of RTT rats paralleled the effects of muscimol application in normal rats. For example, spike rates were not significantly different between normal and RTT rats. This suggests that if excessive inhibition is indeed an important aspect of RTT, then there are also compensatory mechanisms to keep spike rates in a normal range. Such compensatory mechanisms are a well known challenge of studying long term E/I imbalance in neural disorders [81].

Our work highlights the complex role of synchrony in motor system function and dysfunction. We show that MeCP2 disruption can lead to excessive synchrony and a collapse of complexity in the relationships among M1 neurons and the relationships between M1

neurons and the body. Our findings suggest that stereotypy at the level of motor coding may play an important role in the stereotyped body movements of Rett syndrome.

Bibliography

[1] S. Yu, T. L. Ribeiro, C. Meisel, S. Chou, A. Mitz, R. Saunders, and D. Plenz, "Maintained avalanche dynamics during task-induced changes of neuronal activity in nonhuman primates." *eLife*, vol. 6, nov 2017.

[2] E. D. Fagerholm, G. Scott, W. L. Shew, C. Song, R. Leech, T. Knöpfel, and D. J. Sharp, "Cortical Entropy, Mutual Information and Scale-Free Dynamics in Waking Mice," *Cerebral Cortex*, pp. 1–8, jul 2016.

[3] W. L. Shew, W. P. Clawson, J. Pobst, Y. Karimipanah, N. C. Wright, and R. Wessel, "Adaptation to sensory input tunes visual cortex to criticality," *Nature Physics*, pp. 1–48, 2015.

[4] W. P. Clawson, N. C. Wright, R. Wessel, and W. L. Shew, "Adaptation towards scale-free dynamics improves cortical stimulus discrimination at the cost of reduced detection," *PLOS Computational Biology*, vol. 13, no. 5, p. e1005574, may 2017.

[5] G. Scott, E. D. Fagerholm, H. Mutoh, R. Leech, D. J. Sharp, W. L. Shew, and T. Knopfel, "Voltage Imaging of Waking Mouse Cortex Reveals Emergence of Critical Neuronal Dynamics," *Journal of Neuroscience*, vol. 34, no. 50, pp. 16 611–16 620, dec 2014.

[6] G. Hahn, A. Ponce-Alvarez, C. Monier, G. Benvenuti, A. Kumar, F. Chavane, G. Deco, and Y. Frégnac, "Spontaneous cortical activity is transiently poised close to criticality," *PLOS Computational Biology*, vol. 13, no. 5, p. e1005543, may 2017.

[7] T. Bellay, A. Klaus, S. Seshadri, and D. Plenz, "Irregular spiking of pyramidal neurons organizes as scale-invariant neuronal avalanches in the awake state," *eLife*, vol. 4, pp. 1–25, 2015.

[8] Y. Karimipanah, Z. Ma, J.-E. K. Miller, R. Yuste, and R. Wessel, "Neocortical activity is stimulus- and scale-invariant." *PloS one*, vol. 12, no. 5, p. e0177396, 2017.

[9] Z. Ma, G. G. Turrigiano, R. Wessel, and K. B. Hengen, "Cortical Circuit Dynamics Are Homeostatically Tuned to Criticality In Vivo," *Neuron*, vol. 104, no. 4, pp. 655–664.e4, 2019.

[10] J. Wilting and V. Priesemann, "25 years of criticality in neuroscience — established results, open controversies, novel concepts," *Current Opinion in Neurobiology*, vol. 58, pp. 105–111, oct 2019.

[11] M. A. Muñoz, "Colloquium: Criticality and dynamical scaling in living systems," *Reviews of Modern Physics*, vol. 90, no. 3, p. 31001, 2018.

[12] W. L. Shew and D. Plenz, "The functional benefits of criticality in the cortex." *The Neuroscientist : a review journal bringing neurobiology, neurology and psychiatry*, vol. 19, no. 1, pp. 88–100, feb 2013.

[13] S. H. Gautam, T. T. Hoang, K. McClanahan, S. K. Grady, and W. L. Shew, "Maximizing Sensory Dynamic Range by Tuning the Cortical State to Criticality," *PLOS Computational Biology*, vol. 11, no. 12, p. e1004576, 2015.

[14] L. Fakhraei, S. H. Gautam, and W. L. Shew, "State-dependent intrinsic predictability of cortical network dynamics," *PLOS ONE*, vol. 12, no. 5, p. e0173658, may 2017.

[15] W. L. Shew, H. Yang, T. Petermann, R. Roy, and D. Plenz, "Neuronal Avalanches Imply Maximum Dynamic Range in Cortical Networks at Criticality," *Journal of Neuroscience*, vol. 29, no. 49, pp. 15 595–15 600, 2009.

[16] W. L. Shew, H. Yang, S. Yu, R. Roy, and D. Plenz, "Information Capacity and Transmission Are Maximized in Balanced Cortical Networks with Neuronal Avalanches," *Journal of Neuroscience*, vol. 31, no. 1, pp. 55–63, jan 2011.

[17] H. Yang, W. L. Shew, R. Roy, and D. Plenz, "Maximal Variability of Phase Synchrony in Cortical Networks with Neuronal Avalanches," *Journal of Neuroscience*, vol. 32, no. 3, pp. 1061–1072, jan 2012.

[18] A. S. Ecker, P. Berens, G. A. Keliris, M. Bethge, N. K. Logothetis, and A. S. Tolias, "Decorrelated Neuronal Firing in Cortical Microcircuits," *Science*, vol. 327, no. 584, pp. 26–31, 2010.

[19] A. Renart, J. de la Rocha, P. Bartho, L. Hollender, N. Parga, A. Reyes, and K. D. Harris, "The Asynchronous State in Cortical Circuits," *Science*, vol. 327, no. 5965, pp. 587–590, jan 2010.

[20] K. D. Harris and A. Thiele, "Cortical state and attention." *Nature reviews. Neuroscience*, vol. 12, no. 9, pp. 509–23, sep 2011.

[21] C. Stringer, M. Pachitariu, N. A. Steinmetz, M. Okun, P. Bartho, K. Harris, M. Sahani, and N. Lesica, "Inhibitory control of correlated intrinsic variability in cortical networks," *eLife*, vol. 5, 2016.

[22] M. Vinck, R. Batista-Brito, U. Knoblich, and J. A. Cardin, "Arousal and Locomotion Make Distinct Contributions to Cortical Activity Patterns and Visual Encoding," *Neuron*, vol. 86, no. 3, pp. 740–754, 2015.

[23] D. Dahmen, S. Grün, M. Diesmann, and M. Helias, "Second type of criticality in the brain uncovers rich multiple-neuron dynamics," *Proceedings of the National Academy of Sciences*, vol. 116, no. 26, pp. 13 051–13 060, jun 2019.

[24] C. van Vreeswijk and H. Sompolinsky, "Chaos in neuronal networks with balanced excitatory and inhibitory activity." *Science (New York, N.Y.)*, vol. 274, no. 5293, pp. 1724–6, dec 1996.

[25] ——, "Chaotic balanced state in a model of cortical circuits." *Neural computation*, vol. 10, no. 6, pp. 1321–71, aug 1998.

[26] S. Denève and C. K. Machens, "Efficient codes and balanced networks," *Nature Neuroscience*, vol. 19, no. 3, pp. 375–382, mar 2016.

[27] B. Doiron, A. Litwin-Kumar, R. Rosenbaum, G. K. Ocker, and K. Josić, "The mechanics of state-dependent neural correlations," *Nature Neuroscience*, vol. 19, no. 3, pp. 383–393, 2016.

[28] T. P. Vogels and L. F. Abbott, "Signal Propagation and Logic Gating in Networks of Integrate-and-Fire Neurons," *Journal of Neuroscience*, vol. 25, no. 46, pp. 10 786–10 795, 2005.

[29] S. Ostojic, "Two types of asynchronous activity in networks of excitatory and inhibitory spiking neurons," *Nature neuroscience*, vol. 17, no. 4, pp. 594–600, 2014.

[30] R. Rosenbaum, M. A. Smith, A. Kohn, J. E. Rubin, and B. Doiron, "The spatial structure of correlated neuronal variability," *Nature neuroscience*, vol. 20, no. 1, pp. 107–114, 2017.

[31] M. Okun and I. Lampl, "Instantaneous correlation of excitation and inhibition during ongoing and sensory-evoked activities." *Nature neuroscience*, vol. 11, no. 5, pp. 535–7, 2008.

[32] M. Wehr and A. M. Zador, "Balanced inhibition underlies tuning and sharpens spike timing in auditory cortex." *Nature*, vol. 426, no. 6965, pp. 442–6, nov 2003.

[33] B. Haider, D. A. McCormick, A. Duque, and A. R. Hasenstaub, "Neocortical network activity in vivo is generated through a dynamic balance of excitation and inhibition." *The Journal of neuroscience : the official journal of the Society for Neuroscience*, vol. 26, no. 17, pp. 4535–45, 2006.

[34] J. Barral and A. D'Reyes, "Synaptic scaling rule preserves excitatory-inhibitory balance and salient neuronal network dynamics," *Nature Neuroscience*, vol. 19, no. 12, pp. 1690–1696, 2016.

[35] J. Wilting and V. Priesemann, "Between Perfectly Critical and Fully Irregular: A Reverberating Model Captures and Predicts Cortical Spike Propagation," *Cerebral Cortex*, vol. 29, no. 6, pp. 2759–2770, jun 2019.

[36] V. Buendía, P. Villegas, S. di Santo, A. Vezzani, R. Burioni, and M. A. Muñoz, "Jensen's force and the statistical mechanics of cortical asynchronous states," *Scientific Reports*, vol. 9, no. 1, pp. 1–13, 2019.

[37] M. Girardi-Schappo, L. Brochini, A. A. Costa, T. T. A. Carvalho, and O. Kinouchi, "Synaptic balance due to homeostatically self-organized quasicritical dynamics," *Physical Review Research*, vol. 2, p. 12042, 2020.

[38] J. Wilting, J. Dehning, J. Pinheiro Neto, L. Rudelt, M. Wibral, J. Zierenberg, and V. Priesemann, "Operating in a reverberating regime enables rapid tuning of network states to task requirements," *Frontiers in Systems Neuroscience*, vol. 12, p. 55, 2018.

[39] N. Brunel, "Dynamics of Sparsely Connected Networks of Excitatory and Inhibitory Spiking Neurons," *Journal of computational neuroscience*, vol. 208, pp. 183–208, 2000.

[40] J. Touboul and A. Destexhe, "Power-law statistics and universal scaling in the absence of criticality," *Physical Review E*, vol. 012413, pp. 1–15, 2017.

[41] S. Song, P. J. Sjöström, M. Reigl, S. Nelson, and D. B. Chklovskii, "Highly nonrandom features of synaptic connectivity in local cortical circuits." *PLoS biology*, vol. 3, no. 3, p. e68, mar 2005.

[42] Y. Yoshimura, J. L. M. Dantzker, E. M. Callaway, D. Souza, and S. L. Tigrscan, "Excitatory cortical neurons form fine-scale functional networks." *Nature*, vol. 433, no. 7028, pp. 868–73, feb 2005.

[43] K. Rajan and L. F. Abbott, "Eigenvalue spectra of random matrices for neural networks," *Physical Review Letters*, vol. 97, no. 18, pp. 2–5, 2006.

[44] D. R. Muir and T. Mrsic-Flogel, "Eigenspectrum bounds for semirandom matrices with modular and spatial structure for neural networks," *Physical Review E - Statistical, Nonlinear, and Soft Matter Physics*, vol. 91, no. 4, pp. 1–9, 2015.

[45] S. Sadeh, R. A. Silver, T. D. Mrsic-Flogel, and D. R. Muir, "Assessing the Role of Inhibition in Stabilizing Neocortical Networks Requires Large-Scale Perturbation of the Inhibitory Population," *Journal of Neuroscience*, vol. 37, no. 49, pp. 12 050–12 067, 2017.

[46] D. B. Larremore, W. L. Shew, E. Ott, F. Sorrentino, and J. G. Restrepo, "Inhibition Causes Ceaseless Dynamics in Networks of Excitable Nodes," *Physical Review Letters*, vol. 112, no. 13, p. 138103, apr 2014.

[47] J. M. Beggs and D. Plenz, "Neuronal Avalanches in Neocortical Circuits," *Journal of Neuroscience*, vol. 23, no. 35, pp. 11 167–11 177, 2003.

[48] ——, "Neuronal Avalanches Are Diverse and Precise Activity Patterns That Are Stable for Many Hours in Cortical Slice Cultures," *Journal of Neuroscience*, vol. 24, no. 22, pp. 5216–5229, 2004.

[49] S.-S. Poil, R. Hardstone, H. D. Mansvelder, and K. Linkenkaer-Hansen, "Critical-state dynamics of avalanches and oscillations jointly emerge from balanced excitation/inhibition in neuronal networks." *The Journal of neuroscience : the official journal of the Society for Neuroscience*, vol. 32, no. 29, pp. 9817–23, jul 2012.

[50] D. B. Larremore, W. L. Shew, and J. G. Restrepo, "Predicting Criticality and Dynamic Range in Complex Networks: Effects of Topology," *Physical Review Letters*, vol. 106, no. 5, pp. 1–4, jan 2011.

[51] V. Agrawal, A. B. Cowley, Q. Alfaori, D. B. Larremore, J. G. Restrepo, and W. L. Shew, "Robust entropy requires strong and balanced excitatory and inhibitory synapses," *Chaos: An Interdisciplinary Journal of Nonlinear Science*, vol. 28, no. 10, p. 103115, oct 2018.

[52] D. B. Larremore, M. Y. Carpenter, E. Ott, and J. G. Restrepo, "Statistical properties of avalanches in networks," *Physical Review E*, vol. 066131, pp. 1–11, 2012.

[53] C. V. Stewart and D. Plenz, "Homeostasis of neuronal avalanches during postnatal cortex development in vitro," *Journal of Neuroscience Methods*, vol. 169, no. 2, pp. 405–416, 2008.

[54] T. L. Ribeiro, M. Copelli, F. Caixeta, H. Belchior, D. R. Chialvo, M. A. Nicolelis, and S. Ribeiro, "Spike avalanches exhibit universal dynamics across the sleep-wake cycle," *PLoS one*, vol. 5, no. 11, 2010.

[55] J. Zierenberg, J. Wilting, and V. Priesemann, "Homeostatic Plasticity and External Input Shape Neural Network Dynamics," *Physical Review X*, vol. 8, no. 3, p. 31018, 2018.

[56] A. Politi, E. Ullner, and A. Torcini, "Collective irregular dynamics in balanced networks of leaky integrate-and-fire neurons," *European Physical Journal: Special Topics*, vol. 227, no. 10-11, pp. 1185–1204, 2018.

[57] J. P. K. Ip, N. Mellios, and M. Sur, "Rett syndrome: insights into genetic, molecular and circuit mechanisms," *Nature Reviews Neuroscience*, vol. 19, no. June, 2018.

[58] A. Banerjee, R. V. Rikhye, V. Breton-Provencher, X. Tang, C. Li, K. Li, C. A. Runyan, Z. Fu, R. Jaenisch, and M. Sur, "Jointly reduced inhibition and excitation underlies circuit-wide changes in cortical processing in Rett syndrome," *Proceedings of the National Academy of Sciences*, vol. 113, no. 46, pp. E7287–E7296, 2016.

[59] G. Calfa, W. Li, J. M. Rutherford, and L. Pozzo-Miller, "Excitation/inhibition imbalance and impaired synaptic inhibition in hippocampal area CA3 of Mecp2 knockout mice." *Hippocampus*, vol. 25, no. 2, pp. 159–68, feb 2015.

[60] V. S. Dani, Q. Chang, A. Maffei, G. G. Turrigiano, R. Jaenisch, and S. B. Nelson, "Reduced cortical activity due to a shift in the balance between excitation and inhibition in a mouse model of Rett Syndrome," *Proceedings of the National Academy of Sciences*, vol. 102, no. 35, pp. 12 560–12 565, 2005.

[61] D. Tropea, E. Giacometti, N. R. Wilson, C. Beard, C. McCurry, D. D. Fu, R. Flannery, R. Jaenisch, and M. Sur, "Partial reversal of Rett Syndrome-like symptoms in MeCP2 mutant mice." *Proceedings of the National Academy of Sciences of the United States of America*, vol. 106, no. 6, pp. 2029–34, feb 2009.

[62] M. Kron, C. J. Howell, I. T. Adams, M. Ransbottom, D. Christian, M. Ogier, and D. M. Katz, "Brain Activity Mapping in Mecp2 Mutant Mice Reveals Functional Deficits

in Forebrain Circuits, Including Key Nodes in the Default Mode Network, that are Reversed with Ketamine Treatment," *Journal of Neuroscience*, vol. 32, no. 40, pp. 13 860–13 872, 2012.

[63] B. B. Averbeck, P. E. Latham, and A. Pouget, "Neural correlations, population coding and computation." *Nature reviews. Neuroscience*, vol. 7, no. 5, pp. 358–66, may 2006.

[64] M. N. Shadlen and W. T. Newsome, "The variable discharge of cortical neurons: implications for connectivity, computation, and information coding." *The Journal of neuroscience : the official journal of the Society for Neuroscience*, vol. 18, no. 10, pp. 3870–96, may 1998.

[65] L. F. Abbott and P. Dayan, "The effect of correlated variability on the accuracy of a population code," *Neural Computation*, vol. 11, no. 1, pp. 91–101, jan 1999.

[66] V. Agrawal, S. Chakraborty, T. Knöpfel, and W. L. Shew, "Scale-change symmetry in the rules governing neural systems," *iScience*, pp. 121–131, jan 2019.

[67] M. Dichter and G. Ayala, "Cellular mechanisms of epilepsy: a status report," *Science*, vol. 237, no. 4811, pp. 157–164, jul 1987.

[68] M. Steriade, *Neuronal Substrates of Sleep and Epilepsy.* Cambridge: Cambridge University Press, 2003.

[69] P. A. Kells, S. H. Gautam, L. Fakhraei, J. Li, and W. L. Shew, "Strong neuron-to-body coupling implies weak neuron-to-neuron coupling in motor cortex," *Nature Communications*, vol. 10, no. 1, p. 1575, dec 2019.

[70] Y. Wu, W. Zhong, N. Cui, C. M. Johnson, H. Xing, S. Zhang, and C. Jiang, "Characterization of Rett Syndrome-like phenotypes in Mecp2-knockout rats," *Journal of Neurodevelopmental Disorders*, vol. 8, 2016.

[71] C. T. Engineer, K. C. Rahebi, M. S. Borland, E. P. Buell, T. M. Centanni, M. K. Fink, K. W. Im, L. G. Wilson, and M. P. Kilgard, "Degraded neural and behavioral processing of speech sounds in a rat model of Rett syndrome," *Neurobiology of Disease*, vol. 83, pp. 26–34, nov 2015.

[72] B. E. Kolb and R. C. Tees, *The cerebral cortex of the rat.* The MIT Press, 1990.

[73] C. Rossant, S. N. Kadir, D. F. Goodman, J. Schulman, M. L. Hunter, A. B. Saleem, A. Grosmark, M. Belluscio, G. H. Denfield, A. S. Ecker *et al.*, "Spike sorting for large, dense electrode arrays," *Nature neuroscience*, vol. 19, no. 4, pp. 634–641, 2016.

[74] M. Pachitariu, N. A. Steinmetz, S. N. Kadir, M. Carandini, and K. D. Harris, "Fast and accurate spike sorting of high-channel count probes with kilosort," *Advances in neural information processing systems*, vol. 29, pp. 4448–4456, 2016.

[75] J. Li and W. L. Shew, "Tuning network dynamics from criticality to an asynchronous state," *PLOS Computational Biology*, vol. 16, no. 9, p. e1008268, 2020.

[76] M. Okun, N. a. Steinmetz, L. Cossell, M. F. Iacaruso, H. Ko, P. Barthó, T. Moore, S. B. Hofer, T. D. Mrsic-Flogel, M. Carandini, and K. D. Harris, "Diverse coupling of neurons to populations in sensory cortex," *Nature*, vol. 521, no. 7553, pp. 511–515, may 2015.

[77] C. Gardella, O. Marre, and T. Mora, "A Tractable Method for Describing Complex Couplings between Neurons and Population Rate," *eneuro*, vol. 3, no. 4, pp. ENEURO.0160–15.2016, jul 2016.

[78] A. Jackson, V. J. Gee, S. N. Baker, and R. N. Lemon, "Synchrony between Neurons with Similar Muscle Fields in Monkey Motor Cortex," *Neuron*, vol. 38, no. 1, pp. 115–125, apr 2003.

[79] E. Torre, P. Quaglio, M. Denker, T. Brochier, A. Riehle, and S. Grun, "Synchronous Spike Patterns in Macaque Motor Cortex during an Instructed-Delay Reach-to-Grasp Task," *Journal of Neuroscience*, vol. 36, no. 32, pp. 8329–8340, aug 2016.

[80] K. Balasubramanian, V. Papadourakis, W. Liang, K. Takahashi, M. D. Best, A. J. Suminski, and N. G. Hatsopoulos, "Propagating Motor Cortical Dynamics Facilitate Movement Initiation," *Neuron*, vol. 106, no. 3, pp. 526–536.e4, may 2020.

[81] S. Nelson and V. Valakh, "Excitatory/Inhibitory Balance and Circuit Homeostasis in Autism Spectrum Disorders," *Neuron*, vol. 87, no. 4, pp. 684–698, 2015.

A Appendices

A.1 Vita

2013	B. S. in System Science, Beijing Normal University
2016	M. S. in System Theory, Beijing Normal University
2016-2021	Graduate Teaching/Research Assistant, University of Arkansas
2021	Ph. D. in Physics (Neuroscience Concentration), University of Arkansas

A.2 Animal protocols

The IACUC approval memoranda are attached as below.

UNIVERSITY OF ARKANSAS

Office of Research Compliance

MEMORANDUM

TO: Dr. Woodrow Shew

FROM: Craig N. Coon, Chairman
Institutional Animal Care and Use Committee

DATE: June 6, 2014

SUBJECT: IACUC APPROVAL
Expiration date: June 30, 2017

The Institutional Animal Care and Use Committee (IACUC) has APPROVED your protocol 14048: "Neural correlates of unconstrained behavior in rat models of autism". Your start date is July 1, 2014

In granting its approval, the IACUC has approved only the information provided. Should there be any further changes to the protocol during the research, please notify the IACUC in writing(via the Modification form) prior to initiating the changes. If the study period is expected to extend beyond June 30, 2017 you must submit a new protocol. By policy the IACUC cannot approve a study for more than 3 years at a time.

The IACUC appreciates your cooperation in complying with University and Federal guidelines involving animal subjects.

CNC/aem

cc: Animal Welfare Veterinarian

Administration Building 210 • 1 University of Arkansas • Fayetteville, AR 72701-1201 • 479-575-4572
Fax: 479-575-3846 • http://vpred.uark.edu/199

UNIVERSITY OF ARKANSAS

Office of Research Compliance

To:	Woodrow Shew
Fr:	Craig Coon
Date:	October 25th, 2017
Subject:	IACUC Approval
Expiration Date:	October 5th, 2020

The Institutional Animal Care and Use Committee (IACUC) has APPROVED your protocol # **18003:** *Neural correlates of unconstrained behavior in rat models of autism (II).*

In granting its approval, the IACUC has approved only the information provided. Should there be any further changes to the protocol during the research, please notify the IACUC in writing (via the Modification form) prior to initiating the changes. If the study period is expected to extend beyond October 5th, 2020 you must submit a newly drafted protocol prior to that date to avoid any interruption. By policy the IACUC cannot approve a study for more than 3 years at a time.

The following individuals are approved to work on this study: Woodrow Shew, Shree Gautam, Jingwen Li, and Patrick Kells. Please submit personnel additions to this protocol via the modification form prior to their start of work.

The IACUC appreciates your cooperation in complying with University and Federal guidelines involving animal subjects.

CNC/tmp